2011

PRESSURE DRIVEN WALL JET FLOW NEAR CHANNEL EXIT AT MODERATE REYNOLDS NUMBER

Md. Abul Kalam Azad

PRESSURE DRIVEN WALL JET FLOW NEAR CHANNEL EXIT AT MODERATE REYNOLDS NUMBER

(Spine title: Moderate Reynolds number pressure driven wall jet)

(Thesis format: Monograph)

by

Md. Abul Kalam Azad

Graduate Program in Faculty of Engineering

Department of Mechanical and Materials Engineering

A thesis submitted in partial fulfillment
of the requirements for the degree of
Master of Engineering Science

The School of Graduate and Postdoctoral Studies
The University of Western Ontario
London, Ontario, Canada

THE UNIVERSITY OF WESTERN ONTARIO
School of Graduate and Postdoctoral Studies

CERTIFICATE OF EXAMINATION

Supervisor

Prof. Roger E. Khayat

Examiners

Prof. R. E. Baddour

Prof. Liying Jiang

Prof. P. Kaloni

The thesis by

Md. Abul Kalam Azad

entitled:

Pressure Driven Wall Jet Flow Near Channel Exit at Moderate Reynolds Number

is accepted in partial fulfillment of the
requirements for the degree of
Master of Engineering Science

Date

Chair of the Thesis Examination Board

ABSTRACT

The wall jet flow driven by a pressure gradient near channel exit at Reynolds Number ranging from the order of 10 to 100, emerging from a two-dimensional channel is examined theoretically in this study. Poiseuille flow conditions are assumed to prevail far upstream from the exit. The problem is solved using the method of matched asymptotic expansions. The small parameter involved in the expansions is the inverse Reynolds number. The flow and pressure fields are obtained as composite expansions by matching the flow in the boundary-layer region near the free surface, flow in the outer layer region near the stationary plate, and the flow in the core region. The fluid is assumed to be Newtonian and it is found that the jet contracts downstream from the channel exit. The influence of inertia on the shape of free surface is emphasized and the boundary layer structure near the free surface is explored. To leading order, the problem is similar to the case of the free jet (Tillett 1968) with different boundary conditions. A similarity solution can be carried out using a similarity function which is then determined by solving a boundary-value problem, where the equation is integrated subject to the boundary conditions and a guessed value of the slope at the origin. The slope is adjusted until reasonable matching is achieved between the solution and the asymptotic condition far from the free surface. The level of contraction is essentially independent of inertia, but the contraction moves further downstream with increasing Reynolds number. The present work provides the correct conditions near exit, which are required to determine the jet structure further downstream. If the jet becomes thin far downstream, a boundary layer formulation can be used with the presently predicted boundary conditions for steady and possibly transient flows.

KEYWORDS

Matched asymptotic analysis, free surface wall jet, channel exit, large Reynolds number.

ACKNOWLEDGEMENTS

The work could not have been completed without the support and help of many people, for which I am very grateful.

I am especially grateful to my supervisor Professor Roger E Khayat for giving me the opportunity to work on the project of free surface wall jet. I am deeply indebted to him for his uninterrupted thoughtfulness and his support for carrying out my present work.

I would also like to thank my colleagues especially my wife Rizwana Amin, for being very helpful to my research work.

Finally, I sincerely want to thank my mother Sultana Rajia, my father, Md. Abdul Mannan, my two younger brothers Md. Maruf Haider and Imtiaz Haider and my uncle Md. Iqbal Hossain.

TABLE OF CONTENTS

LIST OF FIGURES

LIST OF SYMBOLS

A_n	Perturbation amplitude
B	Constant
c_1	Constant
c_2	Constant
C_n	Composite expansion operator to $o(\varepsilon^n)$
D	Channel width
E_n	Core expansion operator to $o(\varepsilon^n)$
f_2	Similarity function for the flow in the inner region to $o(\varepsilon^2)$
f_3	Similarity function for the flow in the inner region to $o(\varepsilon^3)$
H_m	Inner expansion operator to $o(\varepsilon^n)$
k	Constant
p	Pressure
p_0	Poiseuille pressure
p_n	Perturbation pressure to $o(\varepsilon^n)$
Re	Reynolds number
u	Streamwise velocity component
U_n	Perturbation streamwise velocity
V	Mean velocity due to the pressure gradient inside the channel
V_n	Eigen function of n^{th} mode
w	Transverse velocity component
W_n	Perturbation transverse component
x_∞	Relaxation length
x_m	Distance from the exit where free surface height is maximum
x_P	Upstream distance from the exit where Poiseuille flow is recovered

x, y, z	Coordinates
α	Constant
β_n	n^{th} eigen value
γ	Inverse Reynolds number
δ	Inner layer thickness
ε	Inverse of the cubic root of Reynolds number
ζ	The height of the free surface
ζ_m	Maximum height of the free surface
ξ, η	Coordinates
θ	Similarity variable
μ	Dynamic viscosity
ν	Kinematic viscosity
ρ	Density
σ	Total stress tensor
ϕ	Inclination angle of the free surface
ψ	Stream function
ψ_0	Poiseuille stream function
ψ_n	Stream function perturbation to $o(\varepsilon^n)$

LIST OF APPENDICES

CHAPTER 1

1. INTRODUCTION

The objective of this study is to examine the influence of driving pressure on the two dimensional steady laminar jet of an incompressible fluid near the channel exit. The basic flow configuration is illustrated schematically in figure 1.1. It shows that a pressure driven wall jet emerges out of the channel and with a contracting free surface outside the channel downstream. The flow near the channel exit is closely examined, and the influence of inertia is emphasized. The asymptotic development of the flow field is taken in terms of the inverse Reynolds number, which is assumed to be ranging from the order of 10 to 100. The jet is assumed to be subject to a constant pressure gradient far upstream. The effect of this pressure gradient on the emerging jet, however, will diminish with distance as viscous effects become dominant over inertia as a result of the wall resistance. In this case, the contracting jet begins to expand (swell) with distance downstream from channel exit.

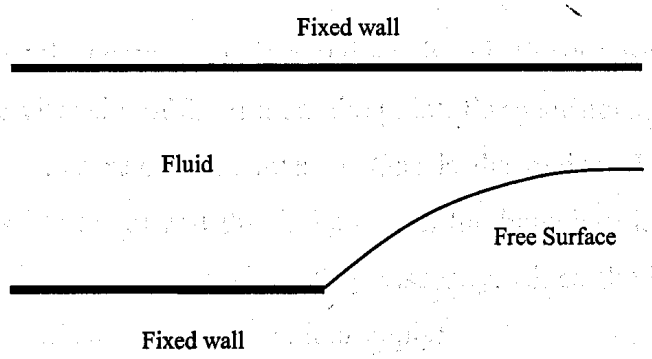

Figure 1.1: Schematic illustration of the basic flow configuration.

1.1 Related flow problems

The literature abounds with prominent works on free jet, wall jet, impinging jet and gravity driven jet. All these problems display an important common behaviour that of boundary layer flow. It is therefore helpful to briefly describe next the concept of boundary layers. The boundary layer equations are perhaps one of the most important advances in fluid dynamics. Using an order of magnitude analysis, the well-known governing Navier–Stokes equations of viscous fluid flow can be greatly simplified within the boundary layer. Notably, the characteristic of the partial differential equations (PDE) becomes parabolic, rather than the elliptical form of the full Navier–Stokes equations. This greatly simplifies the solution of the equations. By making the boundary layer approximation, the flow is divided into an inviscid portion and the boundary layer, which is governed by a PDE. The continuity and Navier–Stokes equations for a two-dimensional steady incompressible flow in indicial form are given by

$$v_{i,i} = 0 \tag{1.1}$$

$$v_j v_{i,j} = -\frac{1}{\rho} p_i + \nu\, v_{i,jj} \tag{1.2}$$

where i and j represents the components in x and y axis, ρ is the density, p is the pressure and ν is the kinematic viscosity of the fluid at the point. For a sufficiently high Reynolds number, there are now two regions of interest. One is the region close to the surface where the viscosity is important and this is known as the boundary layer, and an outer region where the inviscid flow is unaffected by viscosity. Since the boundary layer is generally very thin the following approximations apply:

$$v \ll u \tag{1.3}$$

$$\frac{\partial u}{\partial x} \ll \frac{\partial u}{\partial y} \text{ and } \frac{\partial v}{\partial x} \ll \frac{\partial v}{\partial y} \tag{1.4}$$

Applying the approximation (1.3) and (1.4) into equation (1.2) it is found that

$$\frac{\partial p}{\partial y} \approx 0 \text{ or } p \approx p(x) \tag{1.5}$$

The pressure gradient in x direction can be computed from the Bernoulli's equation which is,

$$\frac{dp}{dx} = -\rho U \frac{dU}{dx} \tag{1.6}$$

Note that, U is the free stream velocity. Finally using (1.3) and (1.4) it can be written that, $\frac{\partial^2 u}{\partial x^2} \ll \frac{\partial^2 u}{\partial y^2}$. Now the two boundary layer equations are written using (1.1) and (1.2):

$$\frac{\partial u}{\partial x} + \frac{\partial v}{\partial y} = 0 \tag{1.7a}$$

$$u\frac{\partial u}{\partial x} + v\frac{\partial u}{\partial y} = U\frac{dU}{dx} + \nu\frac{\partial^2 u}{\partial y^2} \tag{1.7b}$$

The above equations (1.7a) and (1.7b) are the famous boundary-layer equations for a flat plate derived by Prandtl. For a flat plate (figure 1.2) the boundary conditions are the following:

$$\begin{aligned} &\text{At } y = 0 \text{(wall):} && u = v = 0 \quad \text{(no slip)} \\ &\text{At } y = \delta(x): && u = U(x) \end{aligned} \tag{1.8}$$

where $\delta(x)$ is the boundary layer thickness. The next step is to find the similarity solution for the boundary layer equations. A similarity solution is a form of solution in which at least one co-ordinate lacks a distinguished origin; more physically, it describes a flow which 'looks the same' either at all times, or at all length scales. For the laminar flow on the plate, the boundary layer equations (1.7a) and (1.7b) can be solved exactly for u and v. Using co-ordinate transformation, Blasius showed that, the dimensionless velocity profile u/U is a function of η:

$$\frac{u}{U} = f'(\eta) \qquad \eta = y\left(\frac{U}{\nu x}\right)^{1/2} \tag{1.9}$$

Substituting (1.9) into (1.7) the nonlinear PDE problem is reduced to third-order nonlinear ODE for f

$$f''' + \frac{1}{2}ff'' = 0 \tag{1.10}$$

with the boundary conditions

$$\begin{aligned} &\text{At } \eta=0: && f(0)=f'(0)=0 \\ &\text{As } \eta \to \infty: && f'(\infty) \to 1 \end{aligned} \tag{1.11}$$

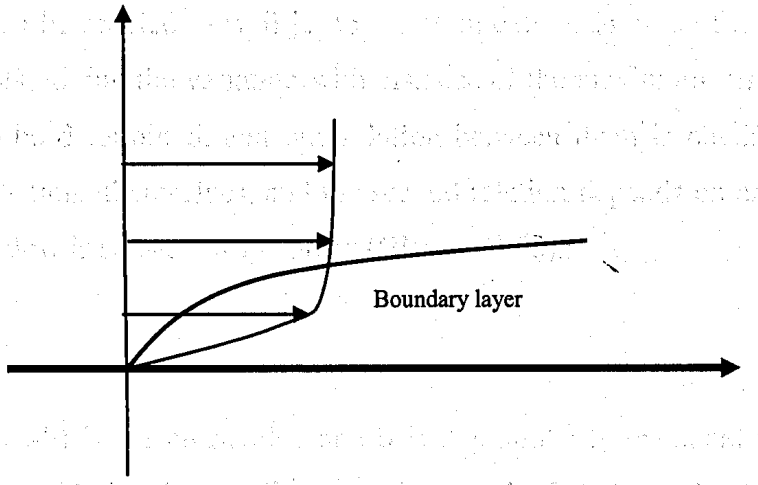

Figure 1.2: Schematic diagram of flat plate boundary layer.

The current problem is closely related to wall jet (Glauert 1956). The relation between the two problems can be understood from figure 1.3. The current problem is included for reference in figure 1.3a. The typical configuration of the more general wall jet is shown in figure 1.3b, where the flow in far field is shown with the fictitious virtual origin (Schlichting 1999). Figure 1.3c shows the analogy between the current problem and the wall jet. The no slip boundary condition on the wall outside the channel is the same for both wall jet and the current problem. The difference between the two problems is in the type of the second boundary condition far from the wall. In the case of the wall jet, the velocity of the fluid becomes zero, while in case of the current problem there is the presence of the free surface on which there is a nonzero velocity of the fluid or slip condition. Note, however, the similarity in velocity profiles in the two cases. Despite the difference in boundary conditions far from the wall, the two velocity profiles display a maximum and decrease with distance. Incidentally, the boundary layer methodology described above can be applied to wall jet to a certain extent. In case of a wall jet, two similarity exponents, giving the variation with distance of the maximum velocity and the jet width, have to be determined, and one relation between them is obtained from the boundary layer equations themselves, and the second relation depends on an eigenvalue, which for laminar flow is satisfactorily solved (Glauert 1956):

$$f''' + ff'' + \alpha f'^2 = 0 \qquad (1.12)$$

where $\alpha = (2b-1)/(2-b)$ is the eigenvalue and b is the similarity exponent related to jet thickness. The value of b for plane wall jet was found to be 3/4. The velocity distribution applies for both radial and plane wall jets. The current problem deals with the free surface wall jet and does not appear to have received attention previously.

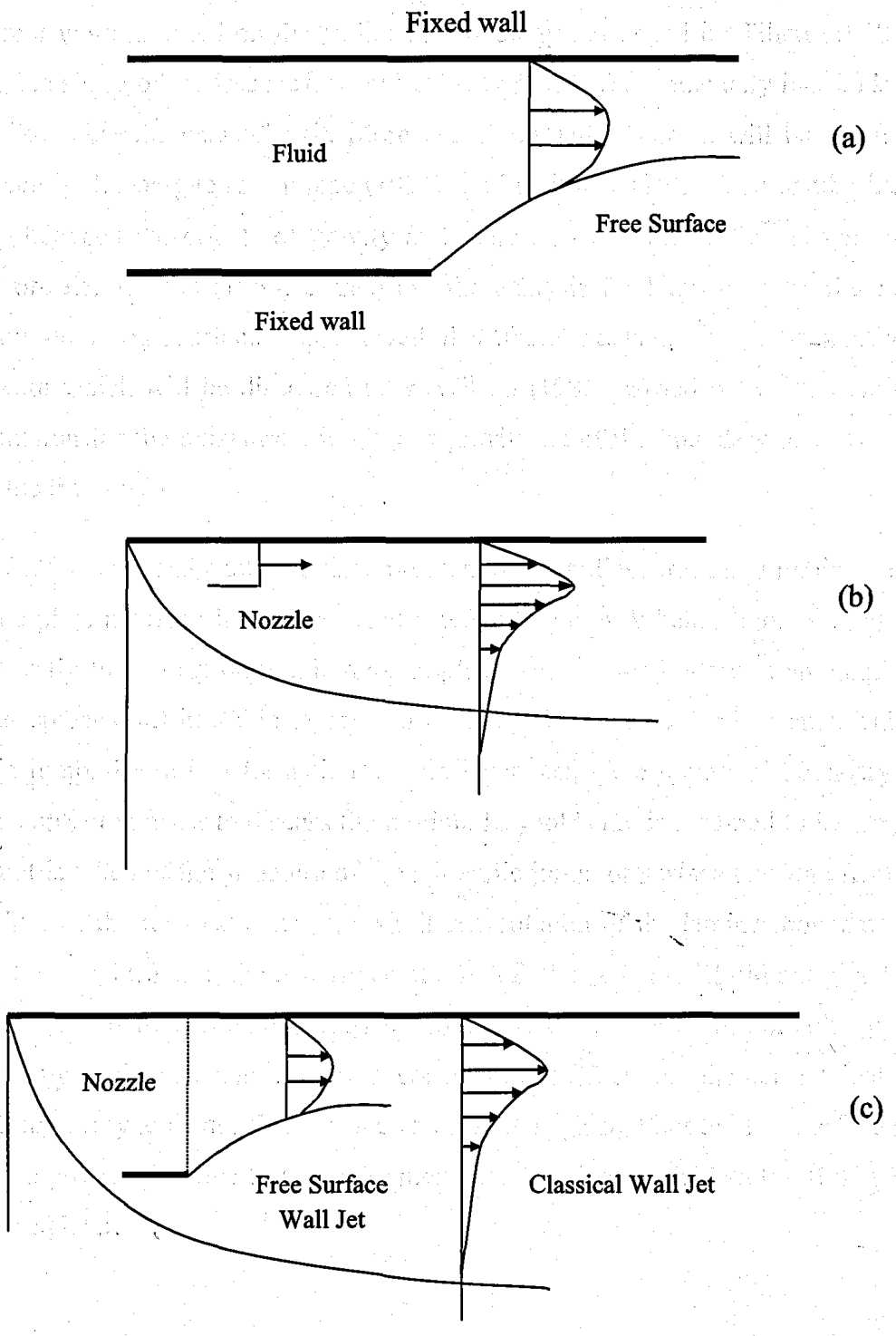

Figure 1.3: Schematic illustration of (a) basic flow configuration, (b) classical wall jet (Glauert 1956), (c) similarity between current problem and classical wall jet flow

The current work is based on the earlier methodology developed by Tillett (1968) who obtained the shape of the free surface and velocity profile for moderately inertial laminar free jet flow near the channel exit. More details on Tillett's work will be given later. More recently, Dumargue & Philippe (1991) used a similar method and emphasized the interplay between the effects of gravity and inertia on the free surface shape and the velocity profile. Watson (1964) carried out the analysis for laminar and turbulent jets impinging on a flat surface and showed that there exists a similarity solution far downstream which will be discussed later. Wilson (1986) carried out a local similarity transformation for the axisymmetric viscous-gravity jet of the boundary layer type flow close to the free surface.

Watson (1964) analyzed another related problem of the radial spread of a liquid jet over a horizontal plate in which he focuses on the hydraulic jump. When a smooth jet of water falls vertically from a tap on to a horizontal plane, such as the bottom of an empty sink, the water spreads out in a thin layer until a sudden increase of depth occurs. This is a hydraulic jump. There is a formation of thin layer inside the jump and boundary-layer theory is applied in order to discuss the motion. Reynolds no. is assumed to be large and no account is taken of the structure of the hydraulic jump, or surface tension effects. For large values of the radial distance r, a similarity solution of the laminar boundary-layer equations is sought. Later, the experimental tests of Watson's model did not give results satisfactorily. Liu & Lienhard (1993) showed that the shape of the circular jump is dominated by surface tension. However, considering the fact that, the current analysis is based on high Reynolds no. flow, surface tension is neglected but the free surface shape can still be predicted correctly using the methodology given by Tillett(1968) which will be discussed later.

1.2 Motivation

Real fluids (liquids and gases included) moving along solid boundary will incur a shear stress on that boundary. As the fluid emerges from a tube or a channel it is subjected to an abrupt change in the shear stress i.e. there is a change in stress from a non-zero value

($\mu\frac{du}{dy}$) to a zero value which causes a singularity to form. This stress singularity constitutes the major difficulty in any theoretical analysis. However, the computational method which seemed to have prevailed over theoretical analysis fails in the case of singularity. The reason of the failure is that, in case of the computational method, the entire flow domain including the singularity and its immediate vicinity must be considered (discretized) and cannot be avoided. The crucial sector to the rest of the flow domain is the singularity region, which is difficult to handle numerically if a satisfactory level of accuracy is sought. In this situation, the asymptotic approach proposed lends itself efficiently as a viable alternative. Perhaps more importantly, asymptotics tend to provide deeper insight on the flow structure near the singularity. The analysis is similar to entry flows where two distinct regions can be identified, an inviscid region and a developing boundary layer that emanates from the entrance point.

For the current free surface wall jet problem at large Reynolds number i.e. low viscosity, the upstream diffusion of vorticity $\left(-\frac{du}{dy}\right)$, which is related to shear stress, is small. The vorticity generated at the leading edge where the stress singularity occurs diffuses depthwise and is convected downstream, ultimately invading the entire flow field. In the inviscid core region, velocity changes occur primarily through conservation of mass. A similar situation occurs for a wall jet at large Reynolds number. For entry flow, the entrance length corresponds to a stress relaxation length, and the inviscid core is replaced with a viscous core in which elongation is small as a result of small axial velocity and stress gradients. For the current problem, velocity gradients in the core region occur primarily because of jet contraction (or expansion depending on the Reynolds number) through conservation of mass. At the exit of the channel, the shear stress drops discontinuously to zero on the free surface. The effect of this drop diffuses toward the wall of the jet both inside (upstream) and outside (downstream) the channel. However, outside the channel, the diffusion is much more significant and is convected downstream, eventually reaching the wall. The original Poiseuille flow gradually acquires a boundary layer character. For a stationary wall, Watson's (1964) similarity solution applies far

downstream where the flow is entirely of the boundary layer type and the viscous relaxation length depends on the driving pressure gradient.

Free surface and interfacial flows are generally complicated because of the unknown position of the surface or interface. The presence of the stress singularity adds complexity to the problem and solution. In the literature, both analytical and computational solution methodologies have been pursued. Although numerical methods seem to have prevailed over analytical approaches for most flow problems, this is not the case for flows with singularity. A combination of analytical and numerical treatments has also been proposed (Shi, Breuer & Durst 2004). As mentioned earlier, in a computational approach, the entire flow domain must be discretized, including the singularity and its surrounding region, both upstream and downstream from the exit. Higher accuracy is achieved through mesh refinement, which captures more effectively the singularity but leads simultaneously to the presence of stronger flow gradients that are difficult to handle numerically (Pasquali & Scriven 2002). In order to circumvent the difficulty with the unknown free surface, Tsukiji & Takahashi (1987) wrote the flow equations in a curvilinear coordinate system related to the network comprising the streamlines and their orthogonal trajectories. Although this approach simplifies the implementation of the boundary conditions, it complicates the flow equations.

1.3 Asymptotic analysis: A historical perspective

Asymptotic analyses tend to avoid the singularity by identifying two distinct flow regions: a boundary layer region near the free surface, extending but not including the singular point, and a core region where the flow remains close to fully developed. The inclusion of the singularity is not essential in this case given the similarity character of the flow in the boundary layer region. Note again that the boundary layer region extends both upstream and downstream from the singularity. However, although the flow does not remain fully developed as it approaches the exit, the thickness of the boundary layer upstream of the exit is generally small at high Reynolds number, and is often ignored. For the current problem, a third layer arises near the wall. Asymptotic analysis has been

successfully adopted for flows in the visco-capillary range (Goren & Wronski 1966, Ruschak & Scriven 1977, Higgins 1982). Goren & Wronski presents two theoretical approaches for the shape of a jet of Newtonian liquid issuing from a capillary needle into air. One approach is a perturbation analysis about the final state of the jet and other is boundary layer analysis near the point of jet formation. Ruschak & Scriven (1977) used the similar analysis in case of a developing laminar flow in a liquid film issuing from a full slot and descending along a vertical wall and obtained the location free boundary and the curved meniscus profile. Higgins (1982) analyzed the downstream development of film flow on a moving substrate using the asymptotic analysis. More closely to the present problem, asymptotic analysis has been adopted in the visco-inertial range (Tillett 1968, Philippe & Dumargue 1991). In this regard, however, little focus has been on jet flow taking inertia into account. Tillett (1968) analyzed the moderately inertial laminar free jet flow near the channel exit using the method of matched asymptotic expansions. Tillett was able to obtain the asymptotic contraction ratio of the jet far downstream using an integral analysis. The results were in good agreement with the experimental results found by Middleman & Gavis (1961). Consequently, the method of matched asymptotic analysis proved to be a very successful tool in examining the flow structure of the jet near the channel exit. Miyake, Mukai & Iemoto (1979) carried out a similar analysis on a vertical jet of inviscid fluid taking into account gravity effect. They considered far downstream flow regions to match with 'near-exit' flow and thus extended the validity of the methodology described by Tillett (1968) to the far downstream region from the exit. Asymptotic analyses have also been successfully implemented for non-Newtonian flows. See, for instance, the work of Denier & Dabrowski (2004) on boundary layer flow, and the work of Zhao & Khayat (2007) for the spreading of a liquid jet.

Tillett considered a jet of liquid, open to atmosphere, which emerges from a two-dimensional channel in which there is Poiseuille flow far upstream. The method of matched asymptotic expansion (Van Dyke 1964) is used to investigate the problem and the small parameter involved in this expansion is the inverse Reynolds no which is based on the channel width. It is assumed in his paper that, in the asymptotic expansion to the lowest order the flow has the Poiseuille profile. Then he considered how the flow is

modified when the fluid leaves the end of the channel in the form of a jet. Surface tension is ignored in his work. Inside the channel the wall stress is $\mu\frac{du}{dz}$. As the fluid detaches itself from the wall of the channel, the removal of the wall stress causes a boundary layer to form at the free surface. In this layer the parabolic velocity profile of the Poiseuille flow adjusts itself so as to satisfy the condition of zero stress at the free surface. It is assumed in his work that Poiseuille flow everywhere is the proper inviscid limit. According to this assumption, the flow in the interior of the jet is unaffected to lowest order, although it is expected that the boundary layer will induce perturbations to it, and also to the flow upstream in the channel. Consider figure 1.4a for Tillett's problem. The solution is developed in powers of ε, where ε^3 is an inverse Reynolds number, both in the 'inner' (boundary-layer) region and in the 'outer' region of the core; the two expansions are matched by standard procedures. The regions of interests are shown in figure 1.4b

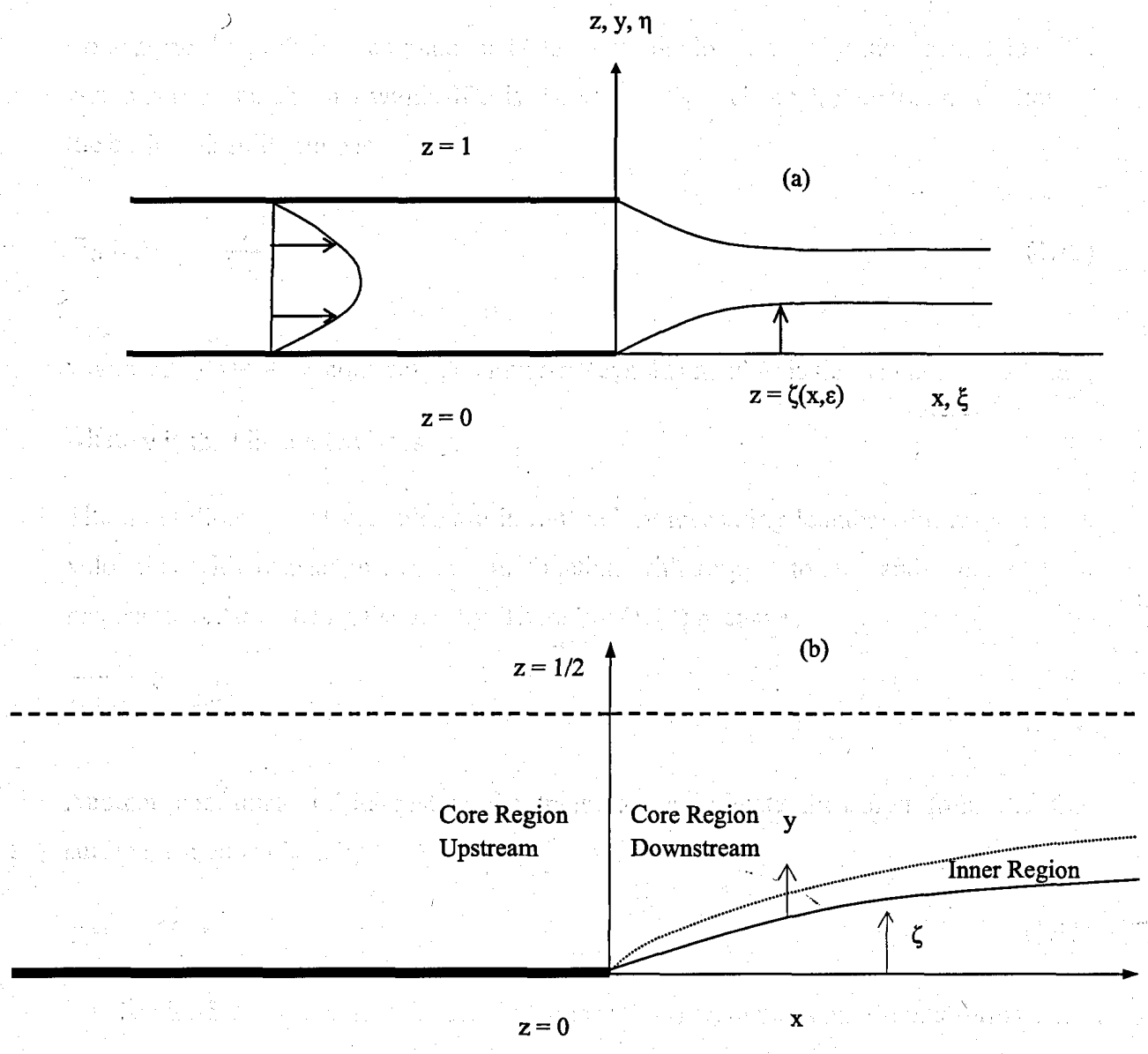

Figure 1.4: Schematic diagram of (a) laminar two dimensional free jet and (b) region of interest in Tillett's work on laminar free jet.

To analyze the problem, the x-axis is taken along the lower edge of the channel, and the z-axis across the channel width. If a is the width of the channel, the stream function of the basic Poiseuille flow is

$$\tilde{\psi}_0 = A(\tilde{z}^2 - \frac{2}{3}\frac{\tilde{z}^3}{a}) \tag{1.13}$$

where $A = \frac{3u_{mean}}{a} =$ constant. The inverse Reynolds number is defined as $\varepsilon_* = \nu / Aa^2$, where ν is the kinematic viscosity.

The non –dimensional variables are introduced by measuring lengths with respect to a, velocities with respect to Aa, stream function with respect to Aa^2 and pressure with respect to $\rho A^2 a^2$, ρ being the density. Therefore (1.13) becomes,

$$\psi_0 = z^2 - \frac{2}{3}z^3 \tag{1.14}$$

Another coordinate of interest is the transverse coordinate measured from the free surface, which is given by

$$y = z - \zeta(x) \tag{1.15}$$

The Navier-Stokes equations for steady laminar flow are, in non-dimensional forms are,

$$\psi_z\psi_{xz} - \psi_x\psi_{zz} = -p_x + \frac{1}{Re}(\psi_{xxz} + \psi_{zzz}) \tag{1.16}$$

$$-\psi_z\psi_{xx} + \psi_x\psi_{xz} = -p_z - \frac{1}{Re}(\psi_{xxx} + \psi_{xzz}) \tag{1.17}$$

In Tillett's work, the problem was solved for large Reynolds number, assuming, nevertheless that the flow remains laminar. For $x > 0$ the boundary conditions that can be applied on the lower free surface $z = \zeta(x)$ are, the kinematic and dynamic boundary conditions. Kinematic boundary conditions means that the free surface itself is the stream

line and dynamic boundary condition means that on the free surface the traction force is zero. These conditions can be written as following

$$\psi = 0 \tag{1.18}$$

$$\vec{t} = \vec{\sigma} \cdot \vec{n} = 0$$

$$\therefore t_x = \sigma_{xx} n_x + \sigma_{xz} n_z = 0 \tag{1.19}$$

and

$$t_z = \sigma_{zx} n_x + \sigma_{zz} n_z = 0$$

where $n_x = \frac{-\zeta'}{\sqrt{\zeta'^2 + 1}}$ and $n_z = \frac{1}{\sqrt{\zeta'^2 + 1}}$. For a Newtonian fluid, total stress is denoted as $\sigma_{ij} = -p\delta_{ij} + \tau_{ij}$ where τ is the shear stress tensor. The dynamic boundary condition then reduces to

$$p + \frac{1}{Re}\left[2\psi_{xz} + \zeta'(\psi_{zz} - \psi_{xx})\right] = 0 \tag{1.19a}$$

$$p\zeta' - \frac{1}{Re}(2\psi_{xz}\zeta' - \psi_{zz} + \psi_{xx}) = 0 \tag{1.19b}$$

The other conditions to be satisfied are,

$$\psi = \frac{1}{6} \text{ on } z = \frac{1}{2} \tag{1.20}$$

$$\psi_z = 0 \text{ on } z = 0,1 \tag{1.21}$$

$$\psi \to z^2 - \tfrac{2}{3}z^3 \text{ as } x \to \infty \tag{1.22}$$

It should be noted that z is considered in the range of $0 \le z \le \frac{1}{2}$; the flow for $\frac{1}{2} \le z \le 1$ is obtained from symmetry considerations.

The boundary layer or inner layer near the free surface is defined as the region where significant deviation occurs from Poiseuille flow. In order to solve the problem in the inner layer, the equations (1.16) and (1.17), and conditions (1.18) and (1.19) are rescaled using the following transformation:

$$x=\xi \text{ and } z=y+\zeta(x),$$

where $y=\varepsilon\eta$, and $\varepsilon=Re^{-\alpha}$ is the small parameter in the problem. Tillett determined α to be equal to 1/3 by balancing inertial and viscous terms in the inner layer. In essence, this transformation "magnifies" the inner layer. In order to match with the outer Poiseuille flow, $\psi \sim y^2$ as $\eta \to \infty$, leading to the following expansion for ψ:

$$\psi(\xi,\eta)=\varepsilon^2\Psi_2(\xi,\eta)+\varepsilon^3\Psi_3(\xi,\eta)+\cdots \tag{1.23}$$

A similarity solution is carried out for Ψ_2 and Ψ_3; which are written here as

$$\Psi_2(\xi,\eta)=\xi^{2/3}f_2(\theta) \text{ and } \Psi_3(\xi,\eta)=\xi f_3(\theta) \tag{1.24}$$

where, $\theta = \eta\xi^{-1/3}$ is the similarity variable used by Goren & Wronski (1966) in his solution and by Goldstein (1930). The equation and boundary conditions for $f_2(\theta)$ and $f_3(\theta)$ are respectively

$$\begin{aligned}
&f_2'''+\frac{2}{3}f_2f_2''-\frac{1}{3}f_2'^2=0,\\
&\text{where } f_2(0)=f_2''(0)=0, \text{ and } f_2(\theta)\sim\theta^2 \text{ as } \theta\to\infty \text{ and}\\
&f_3'''+\frac{2}{3}f_2f_3''-f_2'f_3'+f_2''f_3=0,\\
&\text{where } f_3(0)=f_3''(0)=0, \text{ and } f_3(\theta)\sim -2\theta^3 \text{ as } \theta\to\infty
\end{aligned} \tag{1.25}$$

where the third boundary condition for both $f_2(\theta)$ and $f_3(\theta)$ are found from matching with the core region, which will be discussed later. The boundary conditions at $\theta=0$ reflect the no-penetration and slip condition at the free surface. Tillett found that the surface speed to the order of ε^2 is

$$u(x,y=0)=\varepsilon x^{1/3}f_2'(0)\simeq 2.5572\varepsilon x^{1/3}, \tag{1.26}$$

which confirms the result obtained by Goren & Wronski (1966, equation (28)) to within the 2% accuracy of his calculations. Goren & Wronski (1966) considered the development of such a boundary layer when the basic flow is a simple shear flow and he assumed that the boundary layer does not affect the core flow. However, Tillett did not make this assumption and said that the boundary layer may interact with the core flow. To analyze the flow in the outer region i.e. away from the 'inner' boundary-layer region near z = 0, stream function ψ and pressure p are represented by an outer expansion,

$$\psi(x,z)=\psi_0(x,z)+\varepsilon\psi_1(x,z)+\cdots \tag{1.27a}$$

$$p(x,z)=p_0(x,z)+\varepsilon p_1(x,z)+\cdots \tag{1.27b}$$

Here ψ_0 is just the basic Poiseuille flow. For n = 1, 2 and 3 the equations for $\psi_n(x,z)$ are, from (1.16) and (1.17),

$$\begin{aligned}&\psi_{0z}\psi_{nxz}-\psi_{0zz}\psi_{nx}=-\Pi_{nx}\\&-\psi_{0z}\psi_{nxx}=--\Pi_{nz}\end{aligned} \tag{1.28}$$

where, $\Pi_n(x,z)=p(x,z)+4\varepsilon^3x$. Eliminating Π_n from (1.28) gives

$$\begin{aligned}&\nabla^2\psi_{nx}-\frac{\psi_{0zzz}}{\psi_{0z}}\psi_{nx}=0,\ \text{where}\\&\nabla^2=\frac{\partial^2}{\partial x^2}+\frac{\partial^2}{\partial z^2}\end{aligned} \tag{1.29}$$

Note that, $v=-\psi_{nx}$. From the unique solution of (1.29) for n = 1 and 2 i.e. $v_1(x, z) = v_2(x, z) = 0$, along with the matching between core and inner region, it was found that $\psi_1(x, z) = \psi_2(x, z) = 0$ everywhere. For n =3, a non homogeneous boundary condition is obtained from matching, which is $v_3(x,z\to 0)=-2$. Then, applying the method of separation of variable (see Appendix B) in (1.29) for x < 0, the solution is written as,

$$v_3(x<0,z) = -\psi_{3x}(x<0,z) = -\sum_{n=1}^{\infty} A_n e^{\beta_n x} w_n(z) \tag{1.30a}$$

The coefficients A_n are obtained by matching the flow at the channel exit. Now, the shape functions w_n are governed by the following eigenvalue problem where β_n are the eigenvalues.

$$w_n''(z) + \left(\beta_n^2 + \frac{2}{z-z^2}\right) w_n(z) = 0 \qquad w_n(0) = w_n\left(\frac{1}{2}\right) = 0, \tag{1.30b}$$

Then, using (1.30b) and (1.28) the expressions for pressure inside and outside the channel are obtained as

$$p_3(x<0,z) = -4x - 2\sum_{n=1}^{\infty} \frac{A_n}{\beta_n} e^{\beta_n x} \left\{ \left[z - z^2\right] w_n'(z) - \left[1 - 2z\right] w_n(z) \right\}. \tag{1.31}$$

and

$$p_3(x>0,z) = -2\sum_{n=1}^{\infty} \frac{A_n}{\beta_n} e^{-\beta_n x} \left\{ \left[z - z^2\right] w_n'(z) - \left[1 - 2z\right] w_n(z) \right\}. \tag{1.32}$$

The jet profile or free surface height was sought by Tillett by matching the inner and out solutions (1.23) and (1.27), respectively. As mentioned earlier, matching also allows to obtain the third boundary condition for $f_2(\theta)$ and $f_3(\theta)$, which actually are the matching conditions for Ψ_2 and Ψ_3. In order to match, the following matching rule of Van Dyke (1964) was adopted:

$$E_n H_m \psi = H_m E_n \psi \tag{1.33}$$

Here, E_n is the core-expansion operator, which truncates immediately after the term of order ε^n where the expansion is expressed in terms of core variables. H_m is the corresponding inner-expansion operator. Applying n = 0, and m = 2 in (1.33) gives

$$H_2E_0\psi = \varepsilon^2\eta^2 = y^2 \text{ and}$$
$$E_0H_2\psi = E_0(\varepsilon^2\Psi_2) = y^2 \tag{1.34}$$

which leads to the matching condition for $\Psi_2 \sim \theta^2$. Similarly the next matching condition for Ψ_3 is found by applying m = n = 3 in (1.33) which is $\Psi_3 \sim 2\theta^2$. The expansion for free surface height is given as,

$$\zeta(x) = \varepsilon h_0(x) + \varepsilon^2 h_1(x) + \cdots \tag{1.35}$$

Now, considering m = 2 and n = 1 in (1.33) gives $h_0(x) = cx^{1/3}$ and n = m = 3 gives $h_1(x) = \frac{1}{2}B_3x^{2/3}$. The value of the constants c = 0.70798 and B_3 = -2.08913 are found, respectively, from the numerical integration of (1.25) for $f_2(\theta)$ and $f_3(\theta)$. Finally the free surface height is obtained as

$$\zeta(x) = 0.70798\varepsilon x^{1/3} + 1.04457\varepsilon^2 x^{2/3} + O(\varepsilon^3) \tag{1.36}$$

Finally, the composite flow is obtained from the solutions in the inner and core regions, using Van Dyke's rule of composite solution defined by $C_n \equiv (E_n + H_n - E_nH_n)$. In this case, the composite streamwise velocity is given by

$$C_2u = \varepsilon x^{1/3} f_2'(\theta) + \varepsilon^2 x^{2/3} f_3'(\theta) - 2\varepsilon^2 B_{3z} x^{2/3} + O(\varepsilon^3) \tag{1.37}$$

It should be noted that the boundary-layer solution derived in Tillett's paper breaks down at large distances downstream, when the boundary-layer thickness is no longer small compared to the width of the channel.

1.4 Practical relevance

Although most jet flows in reality are related to the free surface jet flow of Tillett, the applications related to the present wall jet problem in this thesis cannot be under estimated. Thus, laminar free surface wall jet flows can be found in particle removal, cooling, and coating processes. Hence, wall jet flow occurs as impinging jet at an angle which is widely used in mechanical manufacturing to remove particles and water droplets from work pieces. Obtaining the best particle removal efficiency has received much attention in the past. The current analysis in this thesis can be used to obtain the pressure and stress distribution on the plate. The mechanism of particle removal is shown in figure 1.5. The three parameters (see figure 1.6) influencing the particle removal efficiency is the pressure of the impinging jet, the impinging distance and the impinging angle (Zhang et al 2002). In some applications, the impinging angle can be small. In this case, the flow on the left hand-side of figure (1.7) resembles the flow on the right-hand side of figure (1.7), which is the current configuration examined in this thesis, as shown in figure 1.1. If, on the other hand, the impinging angle is large, then the current formulation must be modified, but becomes much more complicated since the Poiseuille profile is not the actual profile in the core region in this case. Thus, for small impinging angle, we can simplify this problem as in figure (1.7), by assuming a wall at the exit and make it coherent to the current analysis which will allow the determination of the correct free surface and pressure distribution on the plate to predict the efficiency of the particle removal from the surface. The case of large impinging angle can be tackled in the future.

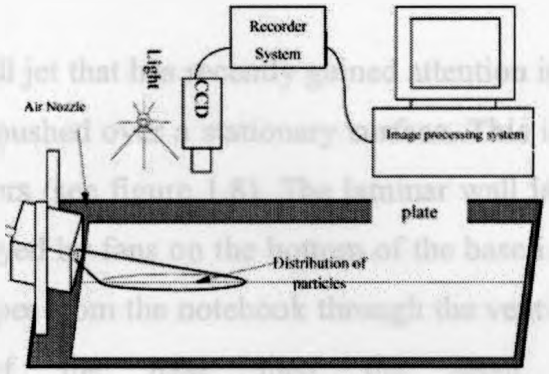

Figure 1.5: Schematic of particle removal setup (Zhang et al 2002).

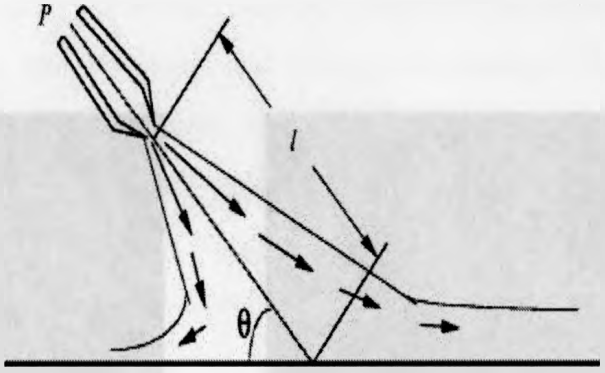

Figure 1.6: The parameters affecting the particle removal efficiency (Zhang et al 2002).

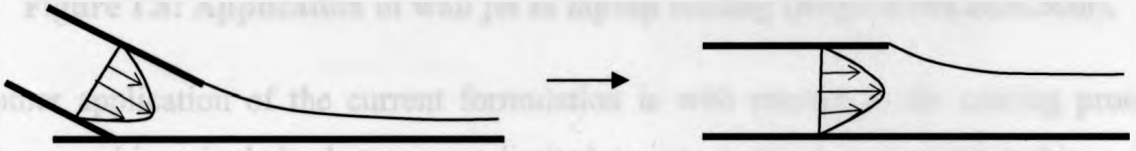

Figure 1.7: Modification of problem of particle removal at an angle to free surface wall jet.

Another application of wall jet that has recently gained attention is in the cooling process when a fluid is driven or pushed over a stationary surface. This is illustrated here in the cooling of laptop processors (see figure 1.8). The laminar wall jet makes the air sucked inside the notebook conveyed by fans on the bottom of the base i.e. the part that rests on the legs. The air then escapes from the notebook through the ventilation grills, located on the opposite side of the base than the input (*http://news.cnet.com, http://www.notebooklist.net/asus-lenovo-and-more/acer-travelmate-8000-timeline-laminar-wall-jet.html*). The theory developed in the thesis can also be extended to thermal problems, although it currently deals only with an isothermal problem.

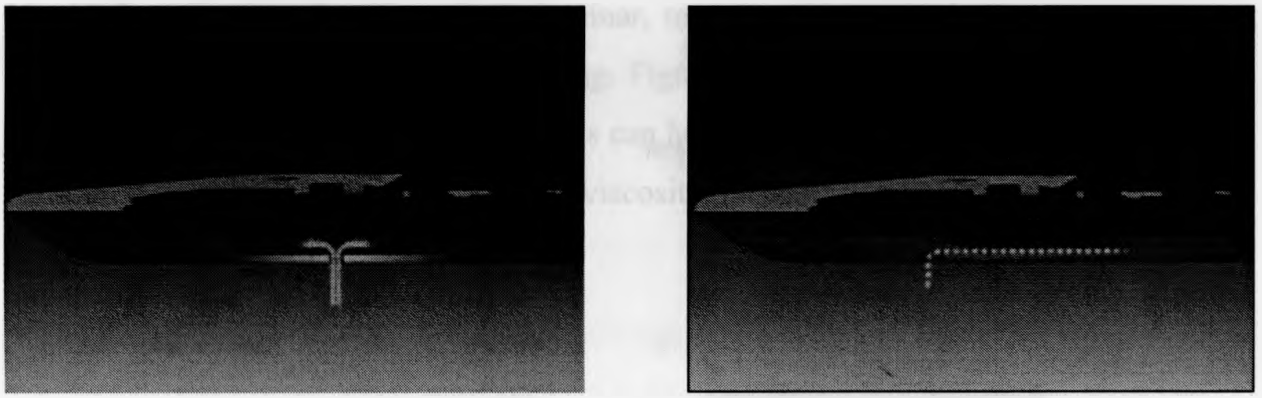

Figure 1.8: Application of wall jet in laptop cooling (http://news.cnet.com).

Another application of the current formulation is with respect to the coating process. Rotary machines include, but are not limited to, gas turbines and steam turbines. The moving part of the turbine is called the rotor while the nonmoving parts i.e. housings, castings etc. are called the stator. Gas or steam leakage, either out of the gas or steam path or into the gas or steam path, from an area of higher pressure to an area of lower pressure, is generally undesirable. In this case, coating is required to provide non-uniform rotor-stator clearance during assembly and operation. The use of spray coating to achieve non-uniform seal clearances in turbomachinary has been patented in by Turnquist et al (2007). The current work in this thesis may be regarded as an alternative to spray coating

in turbomachines. The current work predicts the shape of the emerging jet as it flows on the flat solid plate (substrate). After an initial stage of contraction near the channel exit, the Newtonian film begins to swell and develop a non uniform free surface shape due to weakening of inertia and dominance of viscous dissipation (plate resistance). The current analysis shows how to control the free surface shape by changing the fluid and flow parameters to achieve the desired non uniform coating thickness. Therefore, it can be conjectured that, the current analysis can be a successful application to control the coating thickness and provide the desired non-uniform clearance in turbomachinaries.

Another application involves the manipulation of gas and liquid fluids within networks of microchannels, which is crucial in the design and fabrication of microfluidic devices for applications in microreactors, and chemical and biological sensing (Zhao et al 2001). Liquid flow inside microchannels is laminar, meaning that multiple liquid streams can flow side-by-side without turbulent mixing. Figure 1.9 shows the flow of silane solution into an ambient solvent. The present thesis can help predict the shape of the interface and flow of the emerging jet if the solvent viscosity is negligible compared to that of the silane solution.

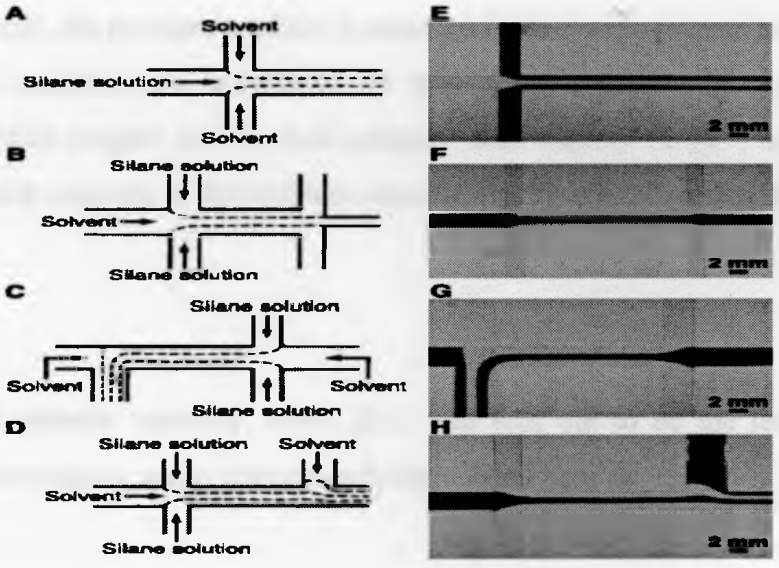

Figure 1.9: Schematic illustrations of multistream laminar flows (A to D) and the corresponding images of aqueous flow inside channels (E to H) (Zhao et al 2001).

CHAPTER 2

2. GENERAL PROBLEM AND BOUNDARY LAYER FLOW

2.1 Governing equations and boundary conditions

Consider the two-dimensional flow of an incompressible fluid of density ρ and viscosity μ, emerging from a channel of width D. The flow configuration is schematically depicted in figure 2.1 in the (X, Z) plane. The X axis is taken along the lower wall and the Z axis is chosen in the transverse direction across the channel. The channel exit coincides with X = 0. The flow is induced by a pressure gradient, dP/dX, inside the channel. The stream function of the basic Poiseuille flow is obtained from

$$\Psi = \frac{1}{2\mu}\frac{dP}{dX}\left(\frac{Z^3}{3} - D\frac{Z^2}{2}\right) = -\frac{6V}{D^2}\left(\frac{Z^3}{3} - D\frac{Z^2}{2}\right) \tag{2.1}$$

where $V = -\frac{1}{12\mu}\frac{dP}{dX}D^2$ is the mean velocity due to the pressure gradient inside the channel. In this case, V is assumed to be always positive and will be used as the velocity scale. In other words, the pressure gradient is assumed to be always present and negative. Non-dimensional variables are introduced by measuring lengths with respect to D, stream function with respect to VD, and pressure with respect to ρV^2. In this case, dimensionless group emerges in the problem, namely, the Reynolds number, Re. Thus,

$$Re = \frac{DV}{\nu} \tag{2.2}$$

where ν is the kinematic viscosity. Now, (2.1) will turn out to be the leading order solution in the outer region, and is conveniently introduced here as

$$\psi_0 = 3z^2 - 2z^3 \tag{2.3}$$

In this study, Re is assumed to be moderately large. The non-dimensional conservation of momentum equation for the laminar steady flow takes the following form

$$\psi_z\psi_{xz} - \psi_x\psi_{zz} = -p_x + \frac{1}{Re}(\psi_{xxz} + \psi_{zzz}) \tag{2.4a}$$

$$-\psi_z\psi_{xx} + \psi_x\psi_{xz} = -p_z - \frac{1}{Re}(\psi_{xxx} + \psi_{xzz}) \tag{2.4b}$$

For $x > 0$, the kinematic and dynamic boundary conditions at the free surface, $z = \zeta(x)$, are

$$\psi = 0 \tag{2.5a}$$

$$p + \frac{1}{Re}\left[2\psi_{xz} + \zeta'(\psi_{zz} - \psi_{xx})\right] = 0 \tag{2.5b}$$

$$p\zeta' - \frac{1}{Re}(2\psi_{xz}\zeta' - \psi_{zz} + \psi_{xx}) = 0 \tag{2.5c}$$

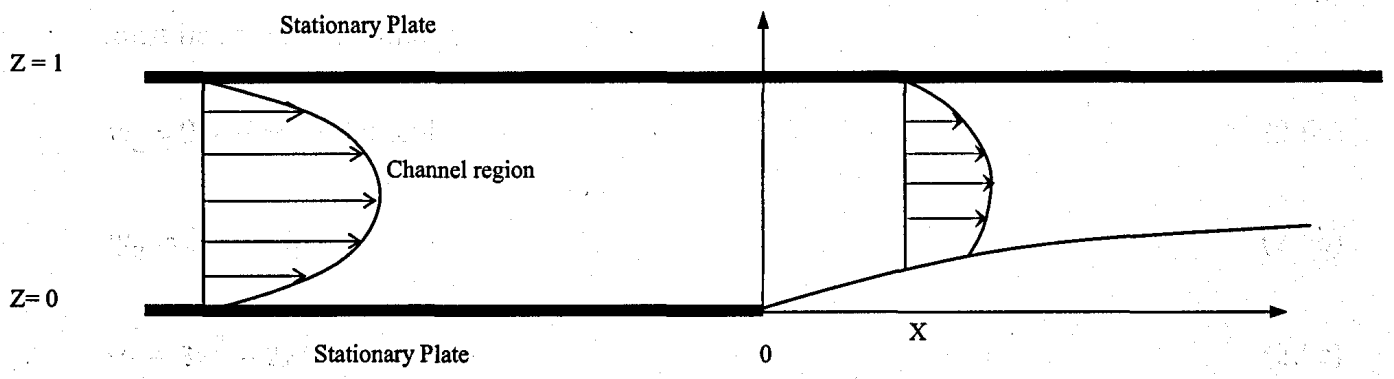

Figure 2.1. Schematic illustration of the planar jet flow. The jet is pressure driven out of the channel. Note that the all notations are dimensional.

A prime denotes total differentiation. Inside the channel ($x < 0$), the following conditions must be satisfied, namely,

$$\psi_z = 0 \text{ and } \psi_x = 0 \text{ at } z=1 \tag{2.6a}$$

$$\psi_z = 0 \text{ at } z=0 \tag{2.6b}$$

$$\psi \to 3z^2 - 2z^3 \text{ as } x \to -\infty \tag{2.6c}$$

The flow is supposed to have the basic Poiseuille profile (2.3) to lowest order and is modified when the fluid leaves the channel in the form of the wall jet. Quoting Tillett(1968), "when the fluid detaches itself from the wall of the channel, the removal of the wall stress causes a boundary layer to form in a region near the free surface. In this region, the parabolic velocity profile adjusts itself so as to satisfy the condition of zero traction at the free surface. In the inviscid limit, this condition would not be imposed since there is no (viscous) mechanism for the stress singularity to diffuse, and all the conditions of the problem would be satisfied by postulating that the parabolic profile continues unchanged in the jet region. However, no uniqueness theorem exists for this inviscid problem, and it is conceivable that other solutions might exist." Nevertheless, it is assumed in this paper that the fully developed Poiseuille flow is everywhere the proper inviscid limit. "With this assumption, the flow in the core of the jet is, to lowest order, not affected by the flow in the boundary layer region" near the free surface although the boundary layer is expected to induce perturbations to the basic Poiseuille flow, when higher order terms are included, both for the flow upstream and downstream from the channel exit. This assumption is similar to the one made by Smith (1979) for the tube flow with severe constriction, where the flow field in the core region, to leading order, satisfy the inviscid equations of motion.

Figure 2.2 illustrates schematically the different flow regions for the free surface wall jet. In each region, different physical mechanisms dominate the flow with corresponding characteristic length scales. In particular, for the flow outside the channel, the region close to the free surface, the inner region, is shear dominated and the flow is of the

boundary layer type. In the region between the interface and the wall, the core region, both shear ($\frac{\partial u}{\partial z}$) and elongation ($\frac{\partial u}{\partial x}$) prevail as a result of the predominance of the Poiseuille character of the flow and the contracting jet. The core region also extends upstream from the exit. At the channel exit, $x = 0$, the shear stress undergoes a step change from a non-zero value(of dimensionless value 6- 12z) at the lower wall, $z = 0$, to zero at the free surface, $z = \zeta(x)$. The effect of this drop diffuses upstream inside the channel ($x < 0$) over a distance x_0 where fully developed Poiseuille flow is recovered, and downstream ($x > 0$) toward the wall over a distance x_∞, at which point the flow is entirely of the boundary layer type. The current study focuses on the flow outside the channel where the similarity solution in the inner region is matched onto the core solution. This latter in turn is matched onto the core solution in the core region inside the channel at the channel exit. Another layer also exists close to the upper wall which is denoted as the outer layer as shown in figure which will be discussed in section 2.3.It is important to observe that no matching is required for the similarity solution at $x = 0$, and the flow singularity at the origin is entirely avoided in the solution process. This constitutes a major advantage of the current formulation compared to alternative solution methods.

The problem is now examined by considering separately the flow near the free surface (inner region), the flow in the core region and the flow near the upper wall i.e. outer region. The composite flow is obtained upon matching the solutions at the interface between the two regions. Part of the formulation in each layer is similar to the free jet formulation carried out by Tillett (1968).

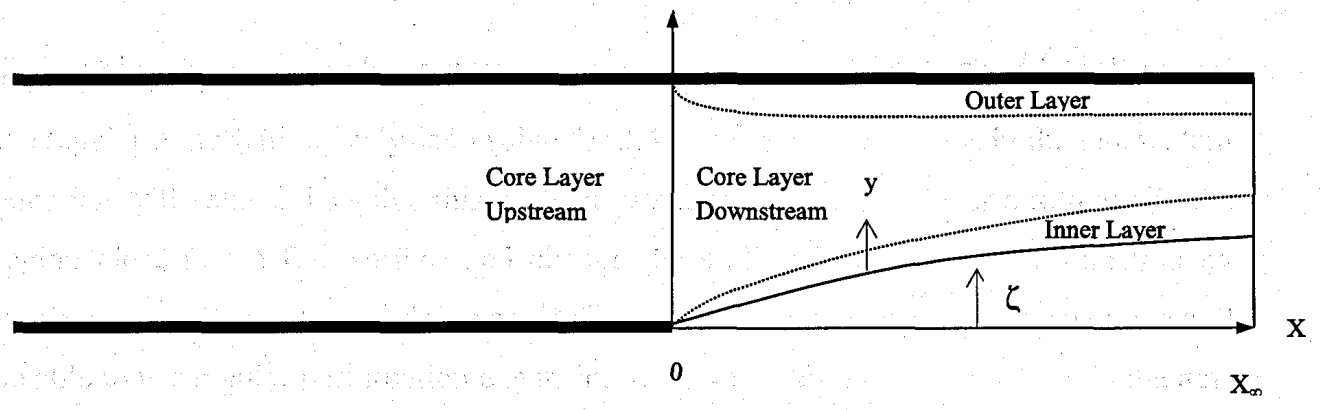

Figure 2.2. Schematic illustration of the computational domain, including the inner, outer and core regions. All notations are dimensionless.

2.2 The flow in the inner layer close to the free surface

To examine the boundary layer structure near the free surface, let $y=z-\zeta(x)$. If we use the regular perturbation analysis to solve for 2.4, the higher order terms in the momentum equation will vanish. To solve this problem we take a small parameter ε to magnify the region close to the free surface and change the scaling in the transverse direction by writing $y=\varepsilon\eta$. It is to be noted that $\varepsilon = Re^{-\alpha}$ and α is to be determined. As a result we will be able to use regular perturbation expansion to solve the momentum equation in the new coordinate system and the higher order terms in the momentum equation will not vanish. Anticipating that the height ζ of the free surface is of the same order of magnitude as the boundary layer thickness, one can write $\zeta(x) = \varepsilon h(x)$, and henceforth work with h. It is not necessary to assume that $h(x) = O(1)$ as $\varepsilon \to 0$; examination of (2.14) below shows that the inner expansion developed in this section holds provided only that $h = o(\varepsilon^{-1})$, i.e. ζ tends to 0 with ε. In the matching process, in chapter 4, it will be shown that $h = O(1)$. Following Tillett (1968), the following change of coordinates is introduced, namely,

$$x=\xi, \qquad z=\varepsilon(\eta+h) \tag{2.7}$$

Now, from (2.4a) and (2.4b), it is concluded that

$$\begin{aligned}\psi_\eta\psi_{\xi\eta}-\psi_\xi\psi_{\eta\eta} &= -\varepsilon^2\left(p_\xi - h'p_\eta\right)+\varepsilon^{\left(\frac{1}{\alpha}-1\right)}\psi_{\eta\eta\eta} \\ &+\varepsilon^{\left(\frac{1}{\alpha}+1\right)}\left(\psi_{\xi\xi\eta}-h''\psi_{\eta\eta}-2h'\psi_{\xi\eta\eta}+h'^2\psi_{\eta\eta\eta}\right)\end{aligned} \tag{2.8a}$$

$$\begin{aligned}-\psi_\eta\psi_{\xi\xi}+\psi_\xi\psi_{\xi\eta}+h''\psi_\eta^2+h'\left(\psi_\eta\psi_{\xi\eta}-\psi_\xi\psi_{\eta\eta}\right) &= -p_\eta \\ -\varepsilon^{\left(\frac{1}{\alpha}-1\right)}\left(\psi_{\xi\eta\eta}-h'\psi_{\eta\eta\eta}\right)-\varepsilon^{\left(\frac{1}{\alpha}+1\right)}\left(\frac{\partial}{\partial\xi}-h'\frac{\partial}{\partial\eta}\right)^3\psi.\end{aligned} \tag{2.8b}$$

Note that ξ and x are distinguished only in differentiation. The aim is to find a solution of these equations in the form of an "inner expansion" in ε. In order to match this to the outer Poiseuille flow, it is necessary to have $\psi \sim y^2$ as $\eta \to \infty$ in the inner region, to lowest order in ε; so ψ must be of order ε^2. In order to determine the value of α, it is required that the convective and viscous terms balance in equations (2.8a) and (2.8b). This is achieved upon taking $\alpha = 1/3$. The components u, the streamwise velocity, and w, the transverse velocity, are now expressed in terms of the stream function as

$$u = \psi_z = \frac{1}{\varepsilon}\psi_\eta \tag{2.9a}$$

$$w = -\psi_x = -\psi_\xi + h'\psi_\eta \tag{2.9b}$$

From (2.9a), it is obvious that u is of order ε. Considering the fact that u in the inner region must match the velocity in the outer region: $u \to 6z - 6z^2$, it is also inferred that u must be of order ε inside the inner region. The order of w can be found using the continuity equation when written in terms of inner variables, or

$$\varepsilon u_\xi - \varepsilon h' u_\eta + w_\eta = 0 \tag{2.10}$$

Thus, w is of order ε^2. The momentum conservation equations can be re-written as

$$\begin{aligned}\psi_\eta\psi_{\xi\eta} - \psi_\xi\psi_{\eta\eta} &= -\varepsilon^2\left(p_\xi - h'p_\eta\right) + \varepsilon^2\psi_{\eta\eta\eta} \\ &+ \varepsilon^4\left(\psi_{\xi\xi\eta} - h''\psi_{\eta\eta} - 2h'\psi_{\xi\eta\eta} + h'^2\psi_{\eta\eta\eta}\right)\end{aligned} \tag{2.11a}$$

$$\begin{aligned}-\psi_\eta\psi_{\xi\xi} + \psi_\xi\psi_{\xi\eta} + h''\psi_\eta^2 + h'\left(\psi_\eta\psi_{\xi\eta} - \psi_\xi\psi_{\eta\eta}\right) &= -p_\eta \\ -\varepsilon^2\left(\psi_{\xi\eta\eta} - h'\psi_{\eta\eta\eta}\right) - \varepsilon^4\left(\frac{\partial}{\partial\xi} - h'\frac{\partial}{\partial\eta}\right)^3\psi\end{aligned} \tag{2.11b}$$

The boundary conditions on the free surface $\eta = 0$ are obtained from (2.5a)-(2.5c) to read

$$\psi = 0 \tag{2.12a}$$

$$\varepsilon\left(h'p+\psi_{\eta\eta}\right)-\varepsilon^3\left[\left(\frac{\partial}{\partial\xi}-h'\frac{\partial}{\partial\eta}\right)^2\psi+2h'\left(\psi_{\xi\eta}-h'\psi_{\eta\eta}\right)\right]=0 \tag{2.12b}$$

$$p+\varepsilon^2\left(2\psi_{\xi\eta}-h'\psi_{\eta\eta}\right)-\varepsilon^4h'\left(\frac{\partial}{\partial\xi}-h'\frac{\partial}{\partial\eta}\right)^2\psi=0 \tag{2.12c}$$

The inner expansion for ψ begins with a term in ε^2. This is assumed, until there is evidence to the contrary. Thus, the expansion proceeds in powers of ε so that

$$\psi(\xi,\eta)=\varepsilon^2\Psi_2(\xi,\eta)+\varepsilon^3\Psi_3(\xi,\eta)+\cdots \tag{2.13}$$

Similarly, h is expanded as

$$h(\xi)=\varepsilon^{-1}\zeta(\xi)=h_0(\xi)+\varepsilon h_1(\xi)+\cdots \tag{2.14}$$

From (2.11)-(2.14), it is concluded that p is of order ε^4. Thus,

$$p(\xi,\eta)=\varepsilon^4P_4(\xi,\eta)+\varepsilon^5P_5(\xi,\eta)+\cdots \tag{2.15}$$

The velocity components are expanded as

$$u(\xi,\eta)=\varepsilon U_1(\xi,\eta)+\varepsilon^2U_2(\xi,\eta)+\cdots \tag{2.16}$$

$$w(\xi,\eta)=\varepsilon^2W_2(\xi,\eta)+\varepsilon^3W_3(\xi,\eta)+\cdots \tag{2.17}$$

In this case, $U_1=\Psi_{2\eta}$, $U_2=\Psi_{3\eta}$ and $W_2=-\Psi_{2\xi}+h'_0\Psi_{2\eta}$, etc.

2.2.1 Flow in the inner region to $O\left(\varepsilon^2\right)$

To leading order, the momentum equation, (2.11a) reads

$$\Psi_{2\eta}\Psi_{2\xi\eta} - \Psi_{2\xi}\Psi_{2\eta\eta} = \Psi_{2\eta\eta\eta} \tag{2.18}$$

The corresponding boundary conditions are obtained from (2.12a) and (2.12b), namely

$$\Psi_2(\xi,0) = \Psi_{2\eta\eta}(\xi,0) = 0 \tag{2.19}$$

To complete the problem for Ψ_2, another boundary condition is required. This is the matching condition, which will be obtained in chapter 4, namely

$$\Psi_2(\xi,\eta) \to 3\eta^2 \text{ as } \eta \to \infty \tag{2.20}$$

Equation (2.18) and conditions (2.19) and (2.20) are similar to the case of a Newtonian jet (Tillett 1968). A similarity solution can be carried out for Ψ_2; which is written here as

$$\Psi_2(\xi,\eta) = \xi^{2/3} f_2(\theta) \tag{2.21}$$

where $\theta = \eta\xi^{-1/3}$ is the similarity variable. The equation for $f_2(\theta)$ is given by

$$3f_2''' + 2f_2 f_2'' - f_2'^2 = 0 \tag{2.22}$$

subject to the following boundary conditions from (2.19) and (2.20):

$$f_2(0) = f_2''(0) = 0 \tag{2.23a}$$

$$f_2(\theta) \sim 3\theta^2 \text{ as } \theta \to \infty \tag{2.23b}$$

An equation similar to (2.22) was investigated by Goldstein (1966) and revisited by Tillett (1968). For large θ, an asymptotic solution is possible to obtain, subject to condition (2.23b), namely

$$f_2(\theta\to\infty)=3(\theta+c_1)^2+O\left[\exp\left(-\frac{2}{3}\theta^3\right)\right] \tag{2.24}$$

where c_1 is a constant determined from the numerical integration. The detail of the asymptotic solution of f_2 is in the appendix A. Problem (2.22)-(2.23) is solved as an initial-value problem, where equation (2.22) is integrated subject to conditions (2.23a) and a guessed value of the slope at the origin. The slope is adjusted until reasonable matching is achieved between the solution and the asymptotic form (2.23b) at large θ, or, more precisely, between f_2'' and 6. The integration is carried out over the domain $[0,\theta_\infty]$, where θ_∞ is a relatively large value of θ where matching is secured to within an imposed tolerance. The value of c_1 is then determined upon matching the numerical solution and its asymptotic counterpart (2.24).

Figure 2.3 displays the dependence of f_2, f_2' and f_2'' on θ. In this figure the curve of f_2 represents the behaviour of the similarity function with respect to the similarity variable θ. Note that, to this order, $u=\varepsilon x^{1/3}f_2'$. Of particular interest is the slope at the origin $f_2'(0)$ which is directly related to the velocity at the free surface. From the figure it is seen that f_2' adjusts itself to behave linearly at shorter distance from origin, while the slope of f_2'' increases linearly very close to origin and then attains a constant value which satisfies the boundary condition $f_2''(\theta\to\infty)\sim 6$. For the purpose of the discussion here, it is convenient to observe that the initial slope is given approximately by $f_2'(0)\sim+5.3$ and the value of c_1 is approximately equal to 0.5. We can conclude from figure 2.3 that the velocity near the free surface increases linearly with height and further downstream the shear stress at the free surface attains a constant value.

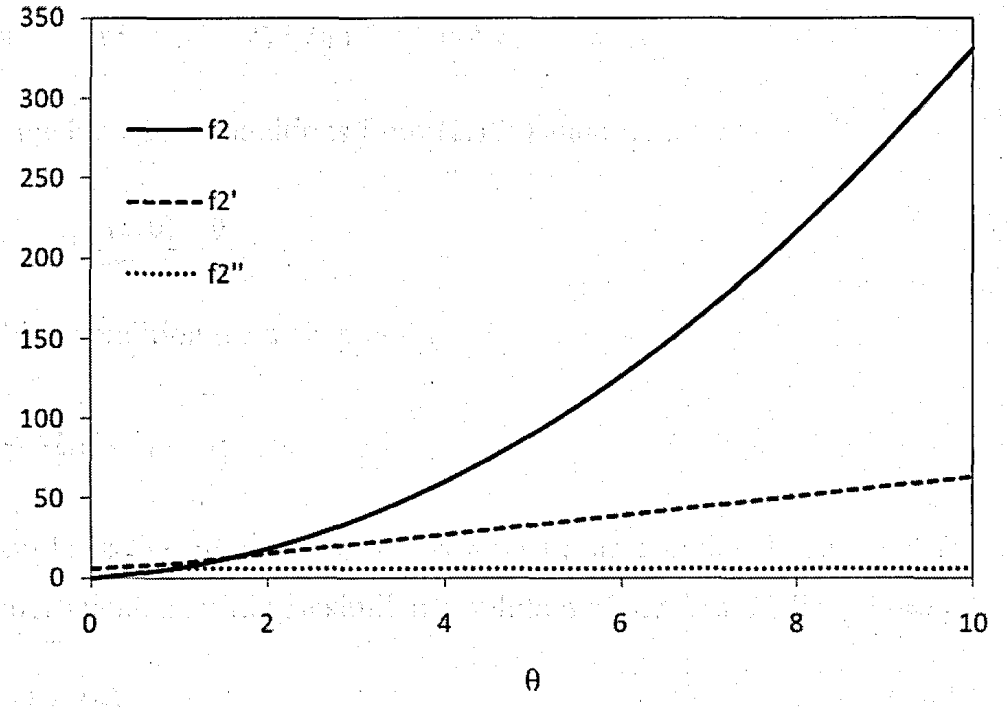

Figure 2.3. Variation of the similarity function f_2 with θ.

2.2.2 Flow in the inner region to $O\left(\varepsilon^3\right)$

To the next order in ε, (2.11a) gives

$$\Psi_{2\eta}\Psi_{3\xi\eta} + \Psi_{3\eta}\Psi_{2\xi\eta} - \Psi_{2\xi}\Psi_{3\eta\eta} - \Psi_{2\eta\eta}\Psi_{3\xi} = \Psi_{3\eta\eta\eta} \tag{2.25}$$

subject to the boundary conditions from (2.12a) and (2.12b), namely

$$\Psi_3(\xi,0) = \Psi_{3\eta\eta}(\xi,0) = 0 \tag{2.26a}$$

The matching condition from chapter 4 is

$$\Psi_3(\xi,\eta) \sim -2\eta^3 \quad \text{as} \quad \eta \to \infty \tag{2.26b}$$

which completes the problem for Ψ_3. Now a linear equation is obtained for Ψ_3, with variable coefficient, admitting a similarity solution of the form (Tillett 1968)

$$\Psi_3(\xi,\eta) = \xi f_3(\theta) \tag{2.27}$$

Substitution of expression (2.27) into equation (2.25) yields the following differential equations for f_3

$$3f_3''' + 2f_2f_3'' - 3f_2'f_3' + 3f_2''f_3 = 0 \tag{2.28}$$

subject to the following boundary conditions:

$$f_3(0) = f_3''(0) = 0 \tag{2.29a}$$

The third boundary condition is obtained from (2.26b):

$$f_3(\theta) \sim -2\theta^3 \quad \text{as} \quad \theta \to \infty \tag{2.29b}$$

An asymptotic solution similar to but more complicated than the case of free jet flow (Tillett 1968) is possible. Thus,

$$f_3(\theta\to\infty)=-2\left[(\theta+c_1)^3-1\right]+c_2(\theta+c_1)+O\left[\exp\left(-2\theta^3\right)\right] \tag{2.30}$$

The numerical integration of equation (2.28) gives the value c_2. The solution procedure is similar to before, except that both problems (2.22)-(2.24) and (2.28)-(2.30) are solved as a coupled system. Figure 2.4 shows the f_3 profile. In this case, f_3 and f_3' are both negative, pointing to a higher order weakening effect on the flow near the free surface. This is seen upon taking the velocity to third order and using expressions (2.16), (2.21) and (2.27), namely

$$u(x,\theta)=\varepsilon x^{1/3}f_2'(\theta)+\varepsilon^2x^{2/3}f_3'(\theta) \tag{2.31}$$

It is deduced from the figure 2.4 that, $f_3'(0)=-5.20$. Thus, the free surface velocity diminishes upon adding the higher order term following

$$u(x,z=\zeta)=5.3\varepsilon x^{1/3}-5.2\varepsilon^2x^{2/3} \tag{2.32}$$

Note that the depthwise velocity component at the free surface will become available once the free surface height is determined. Figure 2.5 illustrates the dependence of free surface velocity on inertia. It displays the $u(x,z=\zeta)$ profiles for ε = 0.1, 0.2, 0.3. Both the figure and equation (2.32) suggest that $u(x,z=\zeta)$ increases monotonically with x. The apparent decrease of the surface velocity with increasing inertia observed in the figure is due to the non-dimensionalization process used. A more suitable scaling for the velocity can be used to reflect the real behaviour. This is reported in figure 2.6, where the $Re\,u(x,z=\zeta)$ profiles (instead of the u profiles) are shown.

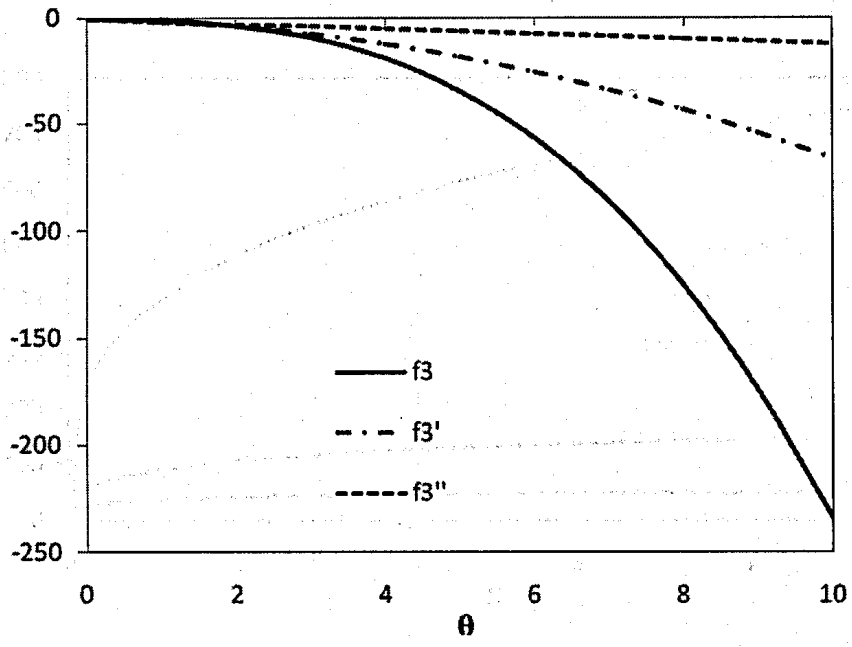

Figure 2.4. Variation of the similarity function f_3 with θ

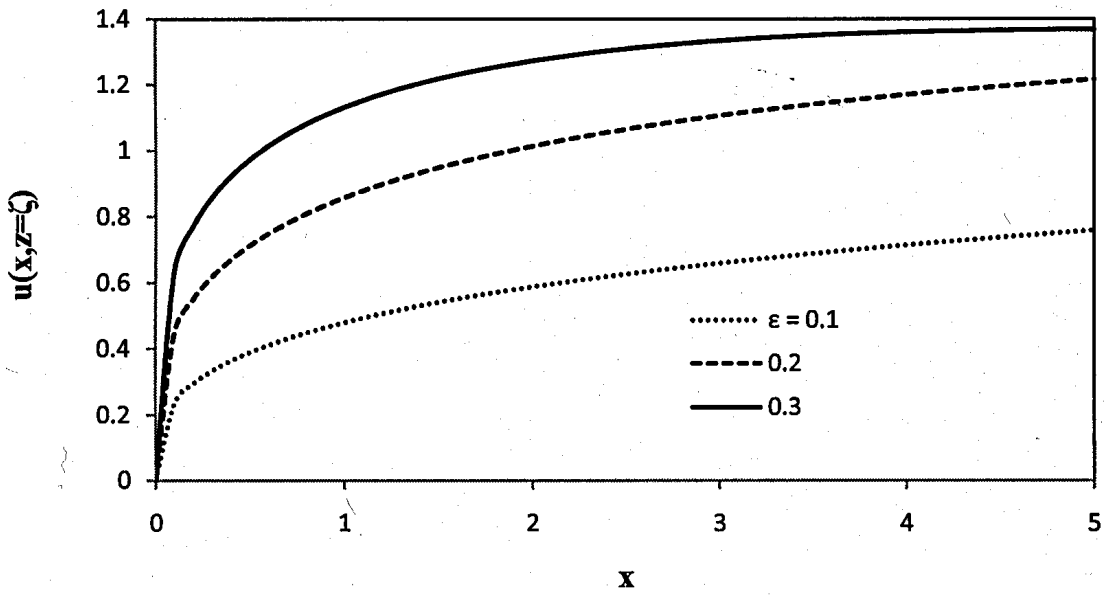

Figure 2.5: Dependence of the nondimensional streamwise velocity at the free surface, $u(x, z = \zeta)$, on inertia for different ε .

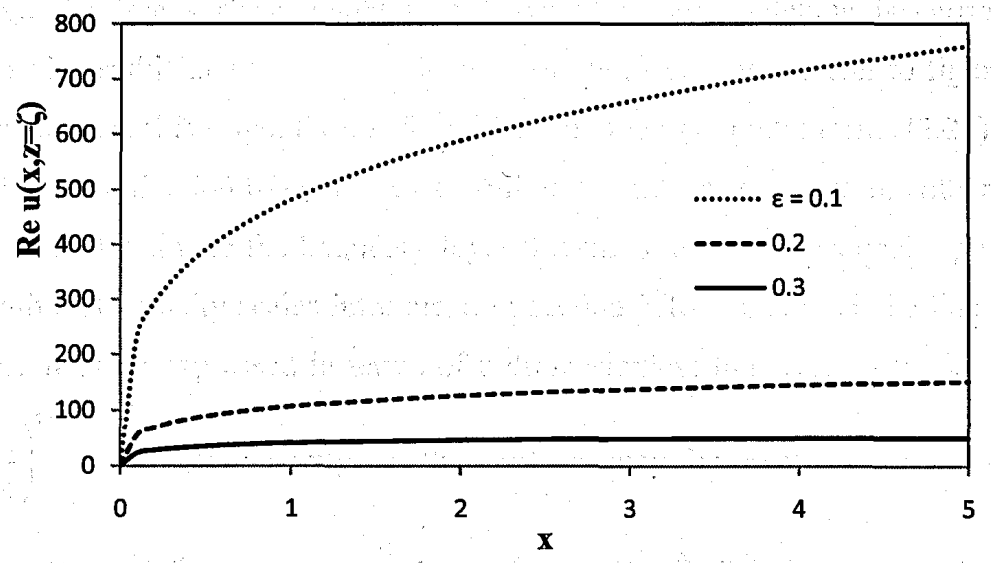

Figure 2.6 : Dependence of the nondimensional streamwise velocity at the free surface, Reu(x, z = ζ), on inertia for different ε .

2.2.3 Boundary layer growth

Although the free surface height is not available until matching is carried out, the boundary layer thickness, $\delta(x)$, or thickness of the inner region (refer to figure 2.2), can be determined at this stage. Expression (2.31) and the asymptotic forms (2.24) and (2.30) allow the determination of $\delta(x)$ and its explicit dependence on ε. On the other hand, it is helpful to first estimate the boundary layer thickness using dimensional arguments, and the length and velocity scales introduced in section 2.1. In this case, the boundary layer thickness may be expressed in terms of a dimensionless transverse diffusion time, t, as $\delta \sim \left(\frac{t}{Re}\right)^{1/2}$, and the velocity at the surface may be expressed in terms of the corresponding axial convection length as $u(x, z=\zeta) \sim \frac{x}{t}$. Eliminating t, and noting from (2.32) that $u(x, z=\zeta) \sim 5.3\varepsilon x^{1/3}$ to leading order, yield the following estimate:

$$\delta(x) \sim \frac{\varepsilon}{\sqrt{5.3}} x^{1/3} = \frac{1}{\sqrt{5.3}} \left(\frac{x}{Re}\right)^{1/3} \tag{2.33}$$

Some important observations can be deduced from the expression above. As expected, the boundary layer thickness grows with position and diminishes with inertia. In comparison with gravity driven jet flow (Wilson 1985), δ behaves like $\left(\frac{x}{Re}\right)^{1/3}$ instead of $\left(\frac{x}{Re}\right)^{1/4}$. In fact, the viscous relaxation length, x_∞, can be estimated upon setting $\delta(x_\infty) = 1$ in expression (2.33), leading to

$$x_\infty = \frac{5.3^{3/2}}{\varepsilon^3} = 5.3^{3/2} Re \tag{2.34}$$

The relaxation length is simply proportional to Re. Note that the (dimensional) Poiseuille shear stresses at the lower wall, - 6V/D from (2.1), is proportional to the corresponding driving velocity, and the resulting jump takes a length to diffuse that is also proportional to V. Interestingly, the actual (dimensional) relaxation length behaves like D^2. For $x > x_\infty$, the boundary layer contains the entire jet width and the nature of the flow depends on the fully developed flow in the channel.

For a more accurate estimate of δ, consider first the variation of the velocity profiles with respect to height, η, at different x position and ε which are displayed in figure 2.7. The figure shows the gradual flattening of the velocity profile near the free surface as inertia decreases. The boundary layer height coincides with the level at which the asymptotic and inner velocity profiles begin to merge, as demonstrated in the figure. The influence of inertia on the boundary layer thickness is illustrated in figure 2.8. The dependence of $\delta(x)$ on ε is shown in this figure. The boundary layer thickness typically grows with position x. Eventually, the inner region continues to grow with position as the film contracts, at which point the boundary layer prevails over the entire film width.

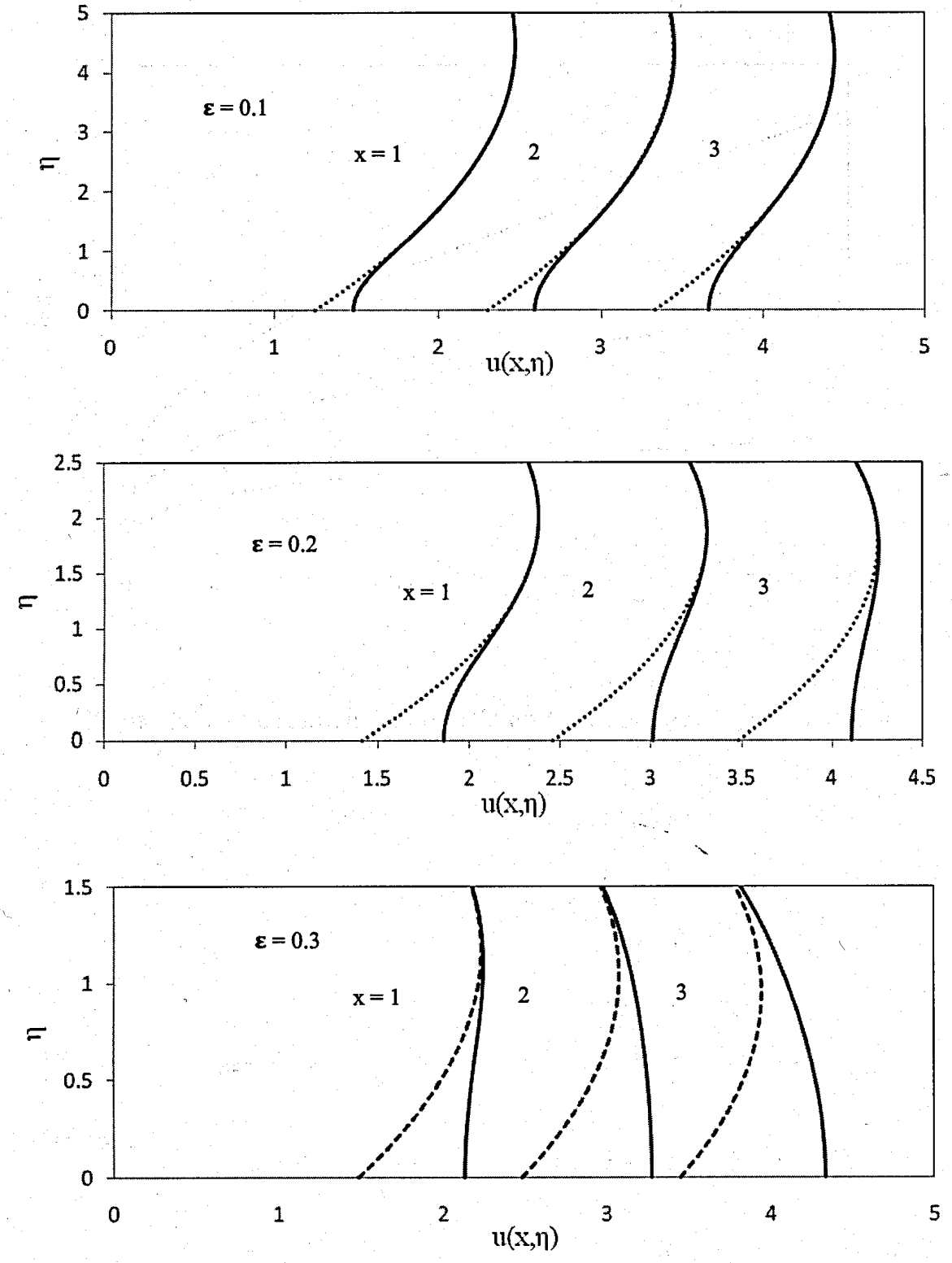

Figure 2.7: Dependence of the streamwise asymptotic (dashed lines), numerical (solid lines) velocity profiles for ε=0.1, 0.2, 0.3, on height η, at x=1, 2, 3

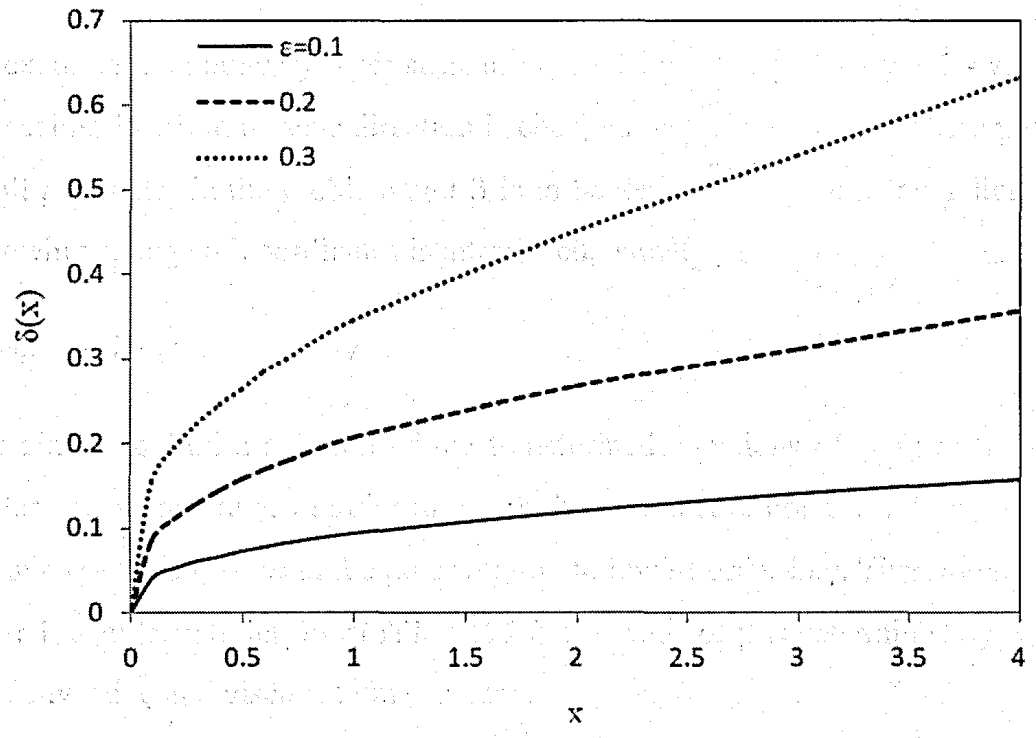

Figure 2.8: The influence of inertia on the boundary layer thickness

2.3 Flow in the outer layer close to the wall

To examine the boundary layer structure near the upper layer, let y = 1 - z. In this case, the scaling in the transverse direction is changed by writing $y = \gamma\eta$, where $\gamma = Re^{-\beta}$ is the small parameter in the problem and β is to be determined. Following Tillett (1968), the following change of coordinates is introduced, namely,

$$x = \xi, \quad z = 1 - \gamma\eta \tag{2.35}$$

The aim is to find a solution of the transformed equations of (2.4) in the form of an "outer expansion" in γ. In order to match this to the core Poiseuille flow, it is necessary to have $\psi \sim 1$ as $\eta \to \infty$ in the outer region, to lowest order in γ. Therefore, ψ must be of order 1. Similarly to jet flow (Tillett 1968), the value of β is determined by requiring that the convective and viscous terms balance.

$$\psi_\eta\psi_{\xi\eta} - \psi_\xi\psi_{\eta\eta} = -\gamma^2 p_\xi - \gamma^{\left(\frac{1}{\beta}-1\right)}\psi_{\eta\eta\eta} - \gamma^{\left(\frac{1}{\beta}+1\right)}\psi_{\xi\xi\eta}, \tag{2.36a}$$

$$\psi_\eta\psi_{\xi\xi} - \psi_\xi\psi_{\xi\eta} = p_\eta - \gamma^{\left(\frac{1}{\beta}-1\right)}\psi_{\xi\eta\eta} - \gamma^{\left(\frac{1}{\beta}+1\right)}\psi_{\xi\xi\xi}. \tag{2.36b}$$

In this case, $\beta = 1$, and $\gamma = \varepsilon^3$. The components u, the streamwise velocity, and w, the transverse velocity, are now expressed in terms of the stream function as

$$u = \psi_z = -\frac{1}{\gamma}\psi_\eta \tag{2.37a}$$

$$w = -\psi_x = -\psi_\xi \tag{2.37b}$$

From (2.37a), it is obvious that u is of order $1/\gamma$. Considering the fact that u in the outer region must match the velocity in the core region: $u \to 6z - 6z^2$, it is also inferred that u must be of order $1/\gamma$ inside the outer region. The order of w can be found using the continuity equation when written in terms of inner variables, or

$$\gamma u_\xi - w_\eta = 0 \tag{2.38}$$

Thus, w is of order 1. The momentum conservation equations (2.36) are re-written as

$$\psi_\eta \psi_{\xi\eta} - \psi_\xi \psi_{\eta\eta} = -\gamma^2 p_\xi - \psi_{\eta\eta\eta} - \gamma^2 \psi_{\xi\xi\eta}, \tag{2.39a}$$

$$\psi_\eta \psi_{\xi\xi} - \psi_\xi \psi_{\xi\eta} = p_\eta - \psi_{\xi\eta\eta} - \gamma^2 \psi_{\xi\xi\xi}. \tag{2.39b}$$

The boundary conditions on the upper flat plate $\eta = 0$ are obtained from (2.6a) to read

$$\psi_\eta = 0 \quad \text{and} \quad \psi(\xi, \eta = 0) = 1 \tag{2.40a}$$

$$\psi(\xi \to -\infty, \eta) = 3(1-\gamma\eta)^2 - 2(1-\gamma\eta)^3. \tag{2.40b}$$

The expansion proceeds in powers of γ so that

$$\psi(\xi,\eta) = \Psi_0(\xi,\eta) + \gamma\Psi_1(\xi,\eta) + \gamma^2\Psi_2(\xi,\eta) + \cdots \tag{2.41}$$

From (2.39), it is concluded that p is of order 1. Thus,

$$p(\xi,\eta) = P_0(\xi,\eta) + \gamma P_1(\xi,\eta) + \gamma^2 P_2(\xi,\eta) + \cdots \tag{2.42}$$

The velocity components are expanded as

$$u(\xi,\eta) = \gamma^{-1} U_{-1}(\xi,\eta) + U_0(\xi,\eta) + \gamma U_1(\xi,\eta) + \cdots \tag{2.43}$$

$$w(\xi,\eta) = W_0(\xi,\eta) + \gamma W_1(\xi,\eta) + \gamma^2 W_2(\xi,\eta) + \cdots \tag{2.44}$$

In this case, $U_{-1} = -\Psi_{0\eta}$, $U_0 = -\Psi_{1\eta}$, $U_1 = -\Psi_{2\eta}$ and $W_0 = -\Psi_{0\xi}$, etc.

To leading order i.e. γ^0, the equation for Ψ_0 and corresponding boundary conditions read

$$\Psi_{0\eta}\Psi_{0\xi\eta} - \Psi_{0\xi}\Psi_{0\eta\eta} = -\Psi_{0\eta\eta\eta}, \tag{2.45a}$$

$$\Psi_{0\eta}\Psi_{0\xi\xi} - \Psi_{0\xi}\Psi_{0\xi\eta} = P_{0\eta} - \Psi_{0\xi\eta\eta} \tag{2.45b}$$

subject to

$$\Psi_{0\eta}(\xi,\eta=0)=0$$

$$\Psi_0(\xi,\eta=0)=\Psi_0(\xi\to-\infty,\eta)=\Psi_0(\xi,\eta\to\infty)=1 \tag{2.40}$$

The last condition is established from matching between the outer and core layers. Clearly, $\Psi_0(\xi,\eta)=1$ is the solution to (2.39a). In this case, (2.39b) gives the result $P_0(\xi,\eta)=P_0(\xi)$, and from matching, one arrives at $P_0(\xi,\eta)=0$. To $O(\gamma)$, the problem is governed by

$$\Psi_{1\eta\eta\eta}=0, \quad P_{1\eta}-\Psi_{1\xi\eta\eta}=0 \tag{2.41}$$

subject to

$$\Psi_{1\eta}(\xi,\eta=0)=0 \qquad \Psi_1(\xi,\eta=0)=0 \tag{2.42a}$$

$$\Psi_1(\xi\to-\infty,\eta)=\Psi_1(\xi,\eta\to\infty)=0 \tag{2.42b}$$

The solution of this problem is $\Psi_1(\xi,\eta)=0$, $P_1(\xi,\eta)=P_1(\xi)$. Although to this order, the flow velocity does not deviate from the Poiseuille flow, there is deviation in the case of the pressure. Indeed, the pressure to this order must match with the pressure in the core layer which, from section 6, gives

$$P_1(\xi)=p_3(x,z=1) \tag{2.43}$$

The explicit form of $p_3(x,z)$ is given by (3.23) and (3.24) for $x < 0$ and $x > 0$, respectively. Next, to $O(\gamma^2)$, one has a similar problem, namely

$$\Psi_{2\eta\eta\eta} = 0,\ P_{2\eta} - \Psi_{2\xi\eta\eta} = 0 \tag{2.44}$$

$$\Psi_2(\xi, \eta = 0) = \Psi_{2\eta}(\xi, \eta = 0) = 0 \tag{2.45a}$$

$$\Psi_2(\xi \to -\infty, \eta) = \Psi_2(\xi, \eta \to \infty) = -3\eta^2 \tag{2.45b}$$

The last condition is arrived at, once again, from matching between the outer and core layers. In this case, at this order, the solution reads: $\Psi_2(\xi,\eta) = -3\eta^2$ and $P_2(\xi\eta) = P_2(\xi)$. Thus, to this order there is no deviation from the fully developed profile for the velocity. In contrast, the pressure continues to depart but remains constant across the outer layer.

2.4 Conclusion

The inner and outer regions were analyzed in this chapter. The aim of the inner region was to find the solution of the equations of motion in the form of an "inner expansion" in ε. The higher order solution was pursued in the inner region in order to achieve the free surface velocity and boundary layer thickness. Similarly, the aim of the analysis of the outer region was to find a solution of the equations of motion in the form of an "outer expansion" in γ. However, to the order of analysis, the outer solution did not provide any significant difference other than the fully developed flow.

CHAPTER 3

3. FLOW IN THE CORE REGIONS

3.1 Core region flow inside and outside the channel

Core region is comprised of the region inside the channel upstream from the exit ($x < 0$) and the region between the inner layer and the outer layer in the downstream ($x > 0$). Ultimately, the flows inside and outside the channel must match at the channel exit ($x = 0$). However, this matching is only required between the two core regions. The reason is that, according to the boundary layer character of the inner regions (inside and outside the channel), similarity solutions can be sought separately. The presence of the singularity at the origin ($x = 0$, $z = 0$) prohibits any matching, but can be totally avoided in the current formulation. In this case, the inner solution inside the channel ($x < 0$) is not required for the determination of the flow outside the channel, and therefore will not be discussed any further.

In the core region (refer to figure 2.2), which is far from the region near $z = 0$, equations (2.4) must be solved, and are conveniently rewritten here as

$$\psi_z\psi_{xz} - \psi_x\psi_{zz} = -p_x + \varepsilon^3\left(\psi_{xxz} + \psi_{zzz}\right) \tag{3.1a}$$

$$-\psi_z\psi_{xx} + \psi_x\psi_{xz} = -p_z - \varepsilon^3\left(\psi_{xxx} + \psi_{xzz}\right) \tag{3.1b}$$

In this case, ψ and p are represented by the following core expansions:

$$\psi(x,z) = \psi_0(x,z) + \varepsilon\psi_1(x,z) + \cdots \tag{3.2a}$$

$$p(x,z) = p_0(x,z) + \varepsilon p_1(x,z) + \cdots \tag{3.2b}$$

Here, recall that $\psi_0 = 3z^2 - 2z^3$ is just the basic Poiseuille flow stream function given in (2.3); ψ_m ($m > 0$) are higher order terms that denote the deviation from the basic flow due to its interaction with the inner and core layer.

The character of the basic flow is similar to that arising for the laminar flow of a free jet (Tillett 1968) and channel or tube flow with constriction (Smith 1976a,b,1979) at high Reynolds number. In those cases, as well, the fully developed (Poiseuille) profile is the flow to leading order. Smith examined the flow for fine, moderate (Smith 1976a,b) and severe (Smith 1979) constrictions. The severity of the constriction is reflected in the characteristic slope of the obstacle, which is of $O(Re^{-1/3})$ and $O(Re^{-1/6})$ for fine and moderate constrictions, respectively. Here Re is Smith's Reynolds number based on the tube diameter and the maximum velocity. In these situations, there occurs virtually no nonlinear upstream influence of the obstacle, and the core flow is just an inviscid rotational perturbation of the basic Poiseuille flow. As it turns out, this is also the situation in the current problem, where the contraction of the flow constitutes a fine to moderate constriction. The core motion outside the inner and outer layers is of the inviscid elliptic, but linear, kind.

In contrast, in a severe constriction, where the obstacle slope is of O(1), there is significant upstream influence on the core flow. As mentioned earlier, this level of constriction severity does not correspond to the current problem. Note that the flow field expansion takes the same form regardless of the constriction level of severity. Thus, Smith's (1979) expansion (2.1) for the flow with severe constriction is the same as the current expansion (3.2) above. However, in contrast to (3.2), Smith's leading order terms in (2.1) do not exactly correspond to fully developed flow, but still satisfy the inviscid equations of motion. Free-streamline theory was adopted by Smith, which is believed to yield the proper inviscid limiting form of the Navier-Stokes equations (Smith 1979). According to Tillett (1968), "since the governing equations are elliptic (in x), this deviation will extend also to the region $x < 0$ in the channel." In other words, the upstream region recognizes the presence of the singularity and free surface.

Based on these assumptions, upon inserting expressions (3.2) into equations (3.1), a hierarchy of equations is obtained to each order. To leading order the resulting equations for m = 0 lead to $p_0(x, z) = 0$. For m = 1, one has

$$\psi_{0z}\psi_{1xz} - \psi_{0zz}\psi_{1x} = -p_{1x} \tag{3.3a}$$

$$-\psi_{0z}\psi_{1xx} = -p_{1z} \tag{3.3b}$$

Upon eliminating p_1 from (3.3a) and (3.3b), the following equation is obtained for ψ_1:

$$\nabla^2\psi_{1x} - \frac{\psi_{0zzz}}{\psi_{0z}}\psi_{1x} = 0 \tag{3.4}$$

where $\nabla^2 = \frac{\partial^2}{\partial x^2} + \frac{\partial^2}{\partial z^2}$. Noting that $w_1 = -\psi_{1x}$, the following boundary-value problem in the ranges $-\infty \le x \le \infty$ and $0 \le z \le 1$ is concluded:

$$\nabla^2 w_1 + \frac{2}{z - z^2} w_1 = 0 \tag{3.5}$$

$$\begin{aligned} &w_1(x,1) = 0, \\ &w_1(x,0) = 0 \qquad \text{for} \quad x < 0, \\ &w_1(x, z \to 0) = -\lambda_1(x) \qquad \text{for} \quad x > 0, \\ &w_1 \quad \text{bounded as } |x| \to \infty. \end{aligned} \tag{3.6}$$

The matching condition obtained in Chapter 4 gives $\lambda_1(x) = 0$. In this case, the (unique) solution to the boundary-value problem (3.5) is $w_1(x, z) = 0$ for any x and z. Consequently, and since $\psi_1(x \to -\infty, z) = 0$, then $\psi_1(x, z)$ and $p_1(x, z)$ must vanish everywhere.

For m = 2, following the similar procedure, w_2 vanishes and consequently $\psi_2(x\ z)$ and $p_2(x, z)$ also vanishes everywhere. More explicitly,

$$\psi_1(x, z) = \psi_2(x, z) = p_1(x, z) = p_2(x, z) = 0 \tag{3.7}$$

To next order, m = 3, equations (2.4) lead to

$$\psi_{0z}\psi_{3xz} - \psi_{0zz}\psi_{3x} = -p_{3x} - 12 \tag{3.8a}$$

$$\psi_{0z}\psi_{3xx} = p_{3z} \tag{3.8b}$$

Upon eliminating p_3 from (3.8a) and (3.8b), the following equation is obtained for ψ_3:

$$\nabla^2\psi_{3x} - \frac{\psi_{0zzz}}{\psi_{0z}}\psi_{3x} = 0 \tag{3.9}$$

Noting again that $w_3 = -\psi_{3x}$, and using expression (2.3) the following boundary value problem in the ranges $-\infty \le x \le \infty$ and $0 \le z \le 1$ is concluded:

$$\nabla^2 w_3 + \frac{2}{z - z^2} w_3 = 0 \tag{3.10a}$$

$$\begin{aligned} &w_3(x,1) = 0, \\ &w_3(x,0) = 0 \qquad \text{for} \quad x < 0, \\ &w_3(x, z \to 0) = -2 \quad \text{for} \quad x > 0, \\ &w_3 \quad \text{bounded as } |x| \to \infty. \end{aligned} \tag{3.10b}$$

The condition $w_3(x > 0, z \to 0) = -2$ is obtained from matching (see Chapter 4). The solution of problem (3.10) does not vanish given the non-homogeneity of the boundary conditions. So far, the formulation in this section has been common to both the regions inside and outside the channel. Although the flow fields in these two regions will have to match at the channel exit (x=0), they can be conveniently examined separately.

3.2 Flow in the core region inside the channel

Consider now the core flow in the region inside the channel ($x < 0$). In this case, using a separation of variable argument (details in Appendix), the solution of problem (3.10) may be written as (Tillett 1968):

$$w_3(x < 0, z) = -\psi_{3x}(x < 0, z) = -\sum_{n=1}^{\infty} A_n e^{\beta_n x} V_n(z) \tag{3.11}$$

The shape functions V_n are governed by the following eigenvalue problem:

$$V_n'' + \left(\beta_n^2 + \frac{2}{z - z^2}\right) V_n = 0 \qquad V_n(0) = V_n(1) = 0, \tag{3.12}$$

An additional boundary condition was required to solve for (3.12) which is $\dot{V_n}(0)=1$. This value is by itself immaterial (as long as it is not zero), and gives the same eigenvalues. However, it will influence the magnitude of the eigenvector. The problem (3.12) was solved using Matlab's ODE45 subroutine. However the boundary conditions cannot be applied at z = 0 and 1 due to the presence of singularity. The eigenvalue was adjusted until the solution converged between the boundary conditions i.e. 0 and 1. The following table shows the eigenvalues that were found for different modes.

n	β_n
1	5.18
2	8.64
3	11.94
4	15.19
5	18.40
6	21.59
7	24.77
8	27.95

Table : Eigenvalues (β_n) for different modes

The equation representing the relation between n and β_n can approximately be written as

$$\beta_n = .0233n^3 - 0.354n^2 + 4.823n + 0.232$$

Figure 3.1(a) depicts the plot of V_n versus z for mode n = 1, 2, 3 and 4. Figure 3.1(b) shows that the Eigen values β_n increases essentially linearly with n.

The stream function inside the channel is obtained by integrating expression (3.11) subject to the boundary condition $\psi_3(x \to -\infty, z) = 0$. This boundary conditions reflects the idea that the core flow far upstream is only basic Poiseuille flow to the leading order. This will lead to

$$\psi(x < 0, z) = 3z^2 - 2z^3 + \varepsilon^3 \sum_{n=1}^{\infty} \frac{A_n}{\beta_n} e^{\beta_n x} V_n(z) \tag{3.13}$$

Finally, the coefficients A_n are obtained by matching the flow at the channel exit, and will therefore be determined once the outer flow is considered for $x > 0$. Figure 3.2 depicts the upstream distance x_p versus ε at which the Poiseuille flow is recovered at different level of z. At first (3.13) is used to find the streamwise velocity u. Then the distance x_p is found when $\text{abs}\left|\frac{u - u_{\text{fully developed}}}{u_{\text{fully developed}}}\right| \leq 10^{-6}$. It can be predicted from the figure that in the upstream for higher inertia fully developed flow is recovered near to exit while for lower inertia the fully developed flow is recovered further from exit. An interesting result can be inferred from the figure that, when the core has reached fully developed flow, it means that the flow at the upper and lower plate region has already reached the fully developed flow.

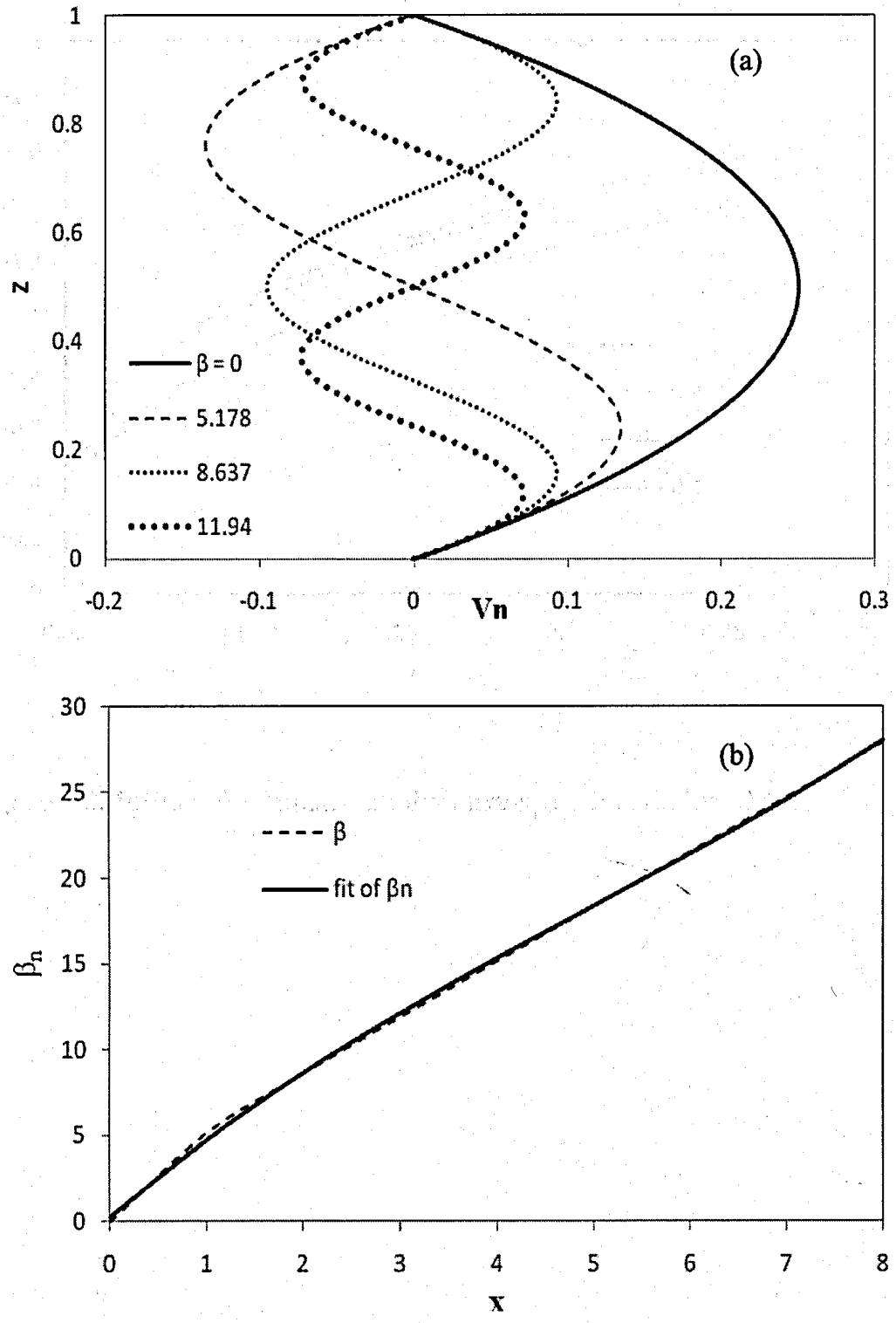

Figure 3.1. Shape function V_n versus z for mode n = 0,1, 2, 3 and 4 shown in (a) and eigenvalues β_n versus n is shown in (b).

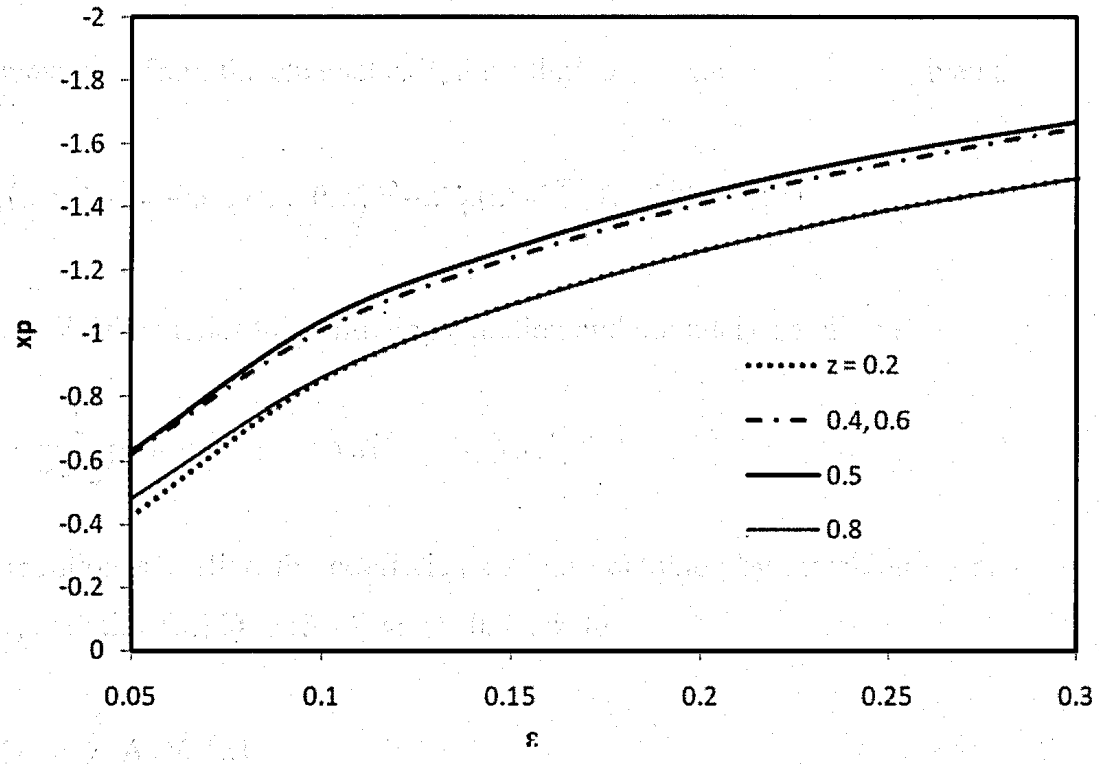

Figure 3.2. Influence of upstream distance x_p on inertia for different height.

3.3 Flow in the core layer outside the channel

Downstream from the channel exit, the solution of problem (3.10) is given as

$$w_3(x>0,z) = -\psi_{3x}(x>0,z) = -2V_0(z) + \sum_{n=1}^{\infty} A_n e^{-\beta_n x} V_n(z) \tag{3.14}$$

where $V_0(z)$ satisfies the following equation and boundary conditions:

$$V_0'' + \frac{2}{z - z^2} V_0 = 0 \qquad V_0(0) = 1,\ V_0(1) = 0 \tag{3.15}$$

As mentioned earlier, the coefficients A_n are obtained by matching w_3 at $x = 0$. In this case, equating (3.11) to (3.14) at $x = 0$, leads to

$$V_0(z) = \sum_{n=1}^{\infty} A_n V_n(z) \tag{3.16}$$

which is a spectral representation of $V_0(z)$ in terms of the orthogonal functions $V_n(z)$. It follows from (3.16), given the orthogonality of the shape functions V_n, that

$$A_n = \frac{\int_0^1 V_0(z) V_n(z) dz}{\int_0^1 V_n^2(z) dz} \tag{3.17}$$

Finally, the stream function is determined upon integrating (3.14) and matching with (3.13) at $x = 0$ to give

$$\psi(x>0,z) = 3z^2 - 2z^3 + \varepsilon^3 \left[2xV_0(z) + \sum_{n=1}^{\infty} \frac{A_n}{\beta_n} e^{-\beta_n x} V_n(z) \right] \tag{3.18}$$

Another variable of vital interest, the pressure, will be discussed next.

3.4 Pressure in the core region and elsewhere

The overall flow inside and outside the channel in the core region can now be examined to provide insight on the flow transition as the fluid nears the channel exit. The pressure inside the channel is determined by integrating equation (3.8b) subject to appropriate boundary conditions, which are obtained as follows. First, recall from section 3 that the pressure in the inner region outside the channel ($x > 0$), was shown to be $O(\varepsilon^4)$. Consequently, upon matching the pressures in the core and inner regions for $x > 0$, it is not difficult to deduce that the pressure in the core region outside the channel vanishes at the interface between the core and inner regions, or

$$p_3(x > 0, z \to 0) = 0 \tag{3.19}$$

Thus, at the channel exit, this gives $p_3(x=0, z\to 0)=0$. Now, upon evaluating (2.3) and (3.11) at $z = 0$, equation (3.8a) reduces to

$$p_{3x}(x < 0, z \to 0) = -12 \tag{3.20}$$

Integrating (3.20) subject to $p_3(0, z\to 0)=0$ gives

$$p_3(x < 0, z \to 0) = -12x \tag{3.21}$$

Upon inserting expressions (2.3) and (3.11) into (3.8b), and using (3.12), the expression for the transverse pressure gradient inside the channel becomes:

$$p_{3z}(x < 0, z) = \left[6z - 6z^2\right]\sum_{n=1}^{\infty} A_n \beta_n e^{\beta_n x} V_n = -\sum_{n=1}^{\infty} \frac{A_n}{\beta_n} e^{\beta_n x}\left\{\left[6z - 6z^2\right]V_n'' + 12V_n\right\} \tag{3.22}$$

which is integrated subject to condition (3.21), leading finally to

$$p_3(x < 0, z) = -12x - \sum_{n=1}^{\infty} \frac{A_n}{\beta_n} e^{\beta_n x}\left\{\left[6z - 6z^2\right]V_n' - [6 - 12z]V_n\right\}. \tag{3.23}$$

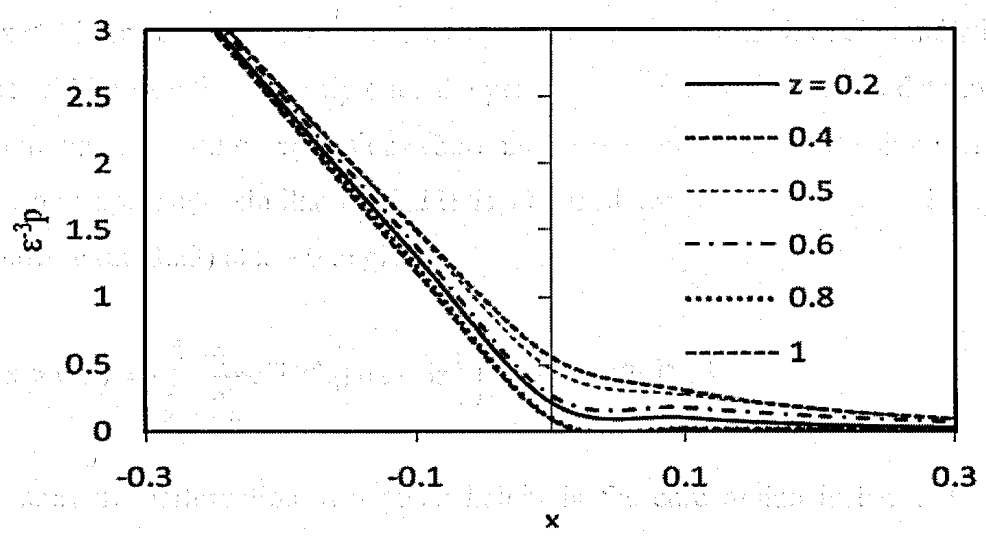

Figure 3.3. Pressure distribution at different height.

Although Poiseuille conditions are theoretically recovered in the limit $x \to -\infty$, calculations based on expression (3.23) indicate that these conditions prevail essentially for $x < -3$, corresponding to a distance approximately equal to three channel widths. This issue will be examined shortly once the pressure outside the channel is determined. This is done upon inserting expressions (2.3) and (3.14) into (3.8b), and using (3.12). In this case, an expression similar to (3.22) is obtained for $x > 0$, which is integrated and matched with (3.23) at $x = 0$ to give

$$p_3(x>0,z) = -\sum_{n=1}^{\infty} \frac{A_n}{\beta_n} e^{-\beta_n x} \left\{ \left[6z - 6z^2 \right] V_n' - [6 - 12z] V_n \right\}. \tag{3.24}$$

The pressure perturbation at a given height in the core region inside and outside the channel is thus given by expressions (3.23) and (3.24), respectively. Incidentally, these expressions are directly involved throughout both the inner and core regions as $\varepsilon^3 p_3(x,z)$ turns out to be equal to the composite pressure (see Chapter 4). In other words, the pressure everywhere is readily available and is given by $p(x,z) \sim \varepsilon^3 p_3(x,z)$. Figure 3.3 illustrates the pressure distribution at different level of z. The pressure decreases monotonically with x and in fact, the pressure remains unaltered by the jet contraction.

3.5 Conclusion

Core region comprises of the region inside the channel upstream from the exit ($x < 0$) and the region between the inner layer and the outer layer in the downstream ($x > 0$) region. After matching these two regions at the channel exit, it is concluded that the core flow deviates from the fully developed Poiseuille flow. The overall flow inside and outside the channel was examined and it is found that the Poiseuille flow is recovered in the upstream to a distance approximately equal to three channel widths.

CHAPTER 4

4. JET PROFILE AND COMPOSITE FLOWS

This section is introduced in order to find out the way how the flow behaves outside the channel. To do this, matching at the interface of the inner and core region is necessary. As there is another region near the upper wall outside the channel, matching is also required between the outer and the core region. However, it is found that, there is no contribution other than the Poiseuille flow from the matching between the outer and core region and thus it will not be discussed in this section. On the other hand by matching between inner and core will give the free surface height.

4.1 Matching at the inner and core interface

The matching rule employed by Van Dyke (1964) is adopted here, namely

$$E_n H_m \psi = H_m E_n \psi \tag{4.1}$$

where m and n are integers. Here, E_n is the core-expansion operator, which truncates immediately after the term of order ε^n where the expansion is expressed in terms of core variables. H_m is the corresponding inner-expansion operator. For successful application of the matching rule (4.1), the stretching transformation between the inner and outer variables must be in the canonical form $y = \varepsilon\eta$. In this case, the core expansion must be written in terms of y, not z; otherwise (4.1) can be satisfied only approximately. It is required that the two expressions in (4.1) be exactly the same, for all m and n.

Different levels of matching (depending on m and n) are needed to obtain the boundary conditions for the inner and core solutions, and consequently to determine the free surface height to each order in ε. The reader is referred to Tillett (1968) for a similar development of the matching process. Initially matching process is implemented to leading order, that is to $O(\varepsilon)$, for the surface height. The details will show later that the matching rule for $m = 2$ and $n = 0$ leads to $\Psi_2 \sim 3\eta^2$ for large η, and, consequently to

(2.20). As to the core solution in chapter 3, the matching with the inner solution for m = 2 and n = 1 leads to $\psi_1(x,0) = \psi_{1x}(x,0) = 0$. These homogeneous conditions in turn lead to the vanishing of ψ_1 everywhere or $\psi_1(x, y) = 0$. The surface height exhibits the same dependence on x as the case of free jet with $c_1 \simeq 0.71$ (Tillett 1968), indicating that a free jet contracts 40% more than a wall jet. Finally, the matching for m = n = 2 leads to $\psi_2(x, y) = 0$. The vanishing of $\psi_1(x, z)$ and $\psi_2(x, z)$ means that, to this order, there is no interaction between the inner layer and the core flow. Similar process will be followed for $O(\varepsilon^2)$.

Recall from (2.3) that, to leading order, the stream function in the outer region is $\psi_0 = 3z^2 - 2z^3$, which can be expressed in terms of $y = z - \zeta$ and h.

$$\psi_0 = 3(y+\varepsilon h)^2 - 2(y+\varepsilon h)^3 \tag{4.2}$$

Consider first m = 2 and n = 0. Applying E_0 on (4.2) gives

$$E_0\psi = 3y^2 - 2y^3 \tag{4.3}$$

As this expression must be in inner variables when the operator H_2 is applied, $E_0\psi$ is rewritten in the form: $E_0\psi = 3\varepsilon^2\eta^2 - 2\varepsilon^3\eta^3$. Therefore,

$$H_2E_0\psi = 3\varepsilon^2\eta^2 = 3y^2 \tag{4.4}$$

To leading order, the inner expansion for the stream function is obtained from (2.13) as $\psi = \varepsilon^2\Psi_2$. Thus $H_2\psi = \varepsilon^2\Psi_2$ and therefore,

$$E_0H_2\psi = E_0(\varepsilon^2\Psi_2). \tag{4.5}$$

This leads to $\Psi_2 \sim 3\eta^2$ for large η, which is condition (2.20) or equivalently (2.23b). Recall that this condition led to the determination of f_2. Consequently, from (2.13), (2.21) and (2.24), at large θ

$$\begin{aligned} H_2\psi &= \varepsilon^2\Psi_2 = \varepsilon^2\xi^{2/3}f_2 = \varepsilon^2\xi^{2/3}3(\theta+c_1)^2 \\ &= \varepsilon^2\xi^{2/3}3\left(\eta\xi^{-1/3}+c_1\right)^2. \end{aligned} \tag{4.6}$$

When (4.6) is expressed in terms of outer variables, it becomes:

$$H_2\psi = 3\left(y+\varepsilon c_1 x^{1/3}\right)^2 = 3\left[y^2+2y\varepsilon c_1 x^{1/3}+\varepsilon^2\left(c_1 x^{1/3}\right)^2\right], \tag{4.7}$$

leading to

$$E_0H_2\psi = 3y^2, \tag{4.8}$$

which matches with (4.4). And again similarly, taking n = 0 and m = 3, leads to

$$H_3E_0\psi = 3\varepsilon^2\eta^2 - 2\varepsilon^3\eta^3 \tag{4.9}$$

Now, $H_3E_0\psi$ must match with $E_0H_3\psi$ and therefore applying H_3 operator on the core expression of ψ,

$$
\begin{aligned}
H_3\psi \quad &= \varepsilon^2\Psi_2 + \varepsilon^3\Psi_3 = \varepsilon^2\xi^{2/3}f_2 + \varepsilon^3\xi f_3(\theta) \\
&= \varepsilon^2\xi^{2/3}3(\theta+c_1)^2 + \varepsilon^3\xi\left[-2\left[(\theta+c_1)^3-1\right]+c_2(\theta+c_1)\right] \\
&= \varepsilon^2\xi^{2/3}3\left(\eta\xi^{-1/3}+c_1\right)^2 + \varepsilon^3\xi\left[-2\left[\left(\eta\xi^{-1/3}+c_1\right)^3-1\right]+c_2\left(\eta\xi^{-1/3}+c_1\right)\right] \\
&= 3\varepsilon^2\xi^{2/3}\left(\eta^2\xi^{-2/3}+2\eta\xi^{-1/3}c_1+{c_1}^2\right) \\
&\quad + \varepsilon^3\xi\left[-2\left(\eta^3\xi^{-1}+3\eta^2\xi^{-2/3}c_1+3\eta\xi^{-1/3}{c_1}^2+{c_1}^3-1\right)+c_2\eta\xi^{-1/3}+c_2c_1\right] \qquad (4.10) \\
&= 3\varepsilon^2\eta^2 + 6\varepsilon^2\eta c_1\xi^{1/3} + 3\varepsilon^2\xi^{2/3}{c_1}^2 \\
&\quad + \varepsilon^3\xi\left[-2\eta^3\xi^{-1}-6\eta^2\xi^{-2/3}c_1-6\eta\xi^{-1/3}{c_1}^2-2{c_1}^3+2+c_2\eta\xi^{-1/3}+c_2c_1\right] \\
&= 3y^2 + 6y\varepsilon c_1\xi^{1/3} + 3\varepsilon^2\xi^{2/3}{c_1}^2 - 2y^3 - 6\varepsilon y^2\xi^{1/3}c_1 - 6\varepsilon^2 y\xi^{1/3}{c_1}^2\xi^{2/3} \\
&\quad - 2\varepsilon^3\xi{c_1}^3 + 2\varepsilon^3\xi + c_2\varepsilon^2 y\xi^{2/3} + c_2c_1\varepsilon^3\xi,
\end{aligned}
$$

which leads to,

$$E_0H_3\psi = 3y^2 - 2y^3 = \varepsilon^2\Psi_2 + \varepsilon^3\Psi_3. \qquad (4.11)$$

Now, (4.11), upon matching with $H_3E_0\psi$, leads to $\Psi_3 \sim -2\eta^3$, and consequently to condition (2.29b).

Next, (4.1) is considered with m = 2 and n = 1. Recall that, the core expansion is $\psi(x,z) = \psi_0(x,z) + \varepsilon\psi_1(x,z) + \cdots$, where $\psi_0 = 3(y+\varepsilon h)^2 - 2(y+\varepsilon h)^3$, therefore, in this case, from (3.2a), (2.4a), (2.7) and (2.14),

$$E_1\psi = 3y^2 - 2y^3 + 6yh_0\varepsilon - 6y^2h_0\varepsilon + \varepsilon\psi_1(x, y+\varepsilon h) \qquad (4.12)$$

Expanding about y, ($\varepsilon h = 0$)

$$\psi_1(x, y+\varepsilon h) = \psi_1(x,y) + \varepsilon h\psi_{1y}(x,y) + \frac{(\varepsilon h)^2}{2}\psi_{1yy}(x,y) \qquad (4.12a)$$

Now, expanding about y = 0

$$\psi_1(x,y+\varepsilon h)=\psi_1(x,0)+y\psi_{1y}(x,0)+\frac{y^2}{2}\psi_{1yy}(x,0)+.....$$
$$+\varepsilon h\psi_{1y}(x,0)+\varepsilon hy\psi_{1yy}(x,0)+..... \qquad (4.12b)$$
$$+\frac{(\varepsilon h)^2}{2}\psi_{1yy}(x,0)+.....$$

As a result, (4.12) reduces to

$$E_1\psi=3y^2-2y^3+6yh_0\varepsilon-6y^2h_0\varepsilon+\varepsilon\psi_1(x,0)$$
$$+\varepsilon y\psi_{1y}(x,0)+\varepsilon\frac{y^2}{2}\psi_{1yy}(x,0) \qquad (4.12c)$$
$$+\varepsilon^2h\psi_{1y}(x,0)+\varepsilon^2hy\psi_{1yy}(x,0).$$

In terms of inner variable, $y=\varepsilon\eta$,

$$E_1\psi=3\varepsilon^2\eta^2-2\varepsilon^3\eta^3+6\varepsilon^2\eta h_0-6\varepsilon^3\eta^2h_0$$
$$+\varepsilon\psi_1(x,0)+\varepsilon^2\eta\psi_{1y}(x,0)+\frac{\varepsilon^3\eta^2}{2}\psi_{1yy}(x,0) \qquad (4.12d)$$
$$+\varepsilon^2h\psi_{1y}(x,0)+\varepsilon^3\eta h\psi_{1yy}(x,0).$$

Therefore, applying H_2 operator,

$$H_2E_1\psi=\varepsilon\psi_1(x,0)+3\varepsilon^2\eta^2+6\varepsilon^2\eta h_0+\varepsilon^2\eta\psi_{1y}(x,0)+\varepsilon^2h\psi_{1y}(x,0)$$
or, (4.13)
$$H_2E_1\psi=\varepsilon\psi_1(x,0)+3y^2+6\varepsilon yh_0+y\varepsilon\psi_{1y}(x,0)+\varepsilon^2h\psi_{1y}(x,0)$$

On the other hand, applying E_1H_2 on the inner expansion (2.13) and using (4.7) give

$$\begin{aligned} H_2\psi &= \varepsilon^2\Psi_2 = \varepsilon^2\xi^{2/3}f_2 = \varepsilon^2\xi^{2/3}3(\theta+c_1)^2 \\ &= \varepsilon^2\xi^{2/3}3\left(\eta\xi^{-1/3}+c_1\right)^2 = 3\varepsilon^2\xi^{2/3}\left(\eta^2\xi^{-2/3}+2\eta\xi^{-1/3}c_1+{c_1}^2\right) \\ &= 3\varepsilon^2\eta^2+6\varepsilon^2\eta c_1\xi^{1/3}+3\varepsilon^2\xi^{2/3}{c_1}^2 \\ &= 3y^2+6y\varepsilon c_1\xi^{1/3}+3\varepsilon^2\xi^{2/3}{c_1}^2 \end{aligned} \tag{4.14a}$$

which leads to upon applying the operator E_1,

$$E_1H_2\psi = 3y^2+6y\varepsilon c_1x^{1/3}. \tag{4.14b}$$

Comparing (4.13) and (4.14b) leads to $\psi_1(x, 0) = 0$. This leads in turn to the homogeneous boundary condition $\lambda_1(x) = -\psi_{1x}(x,0) = 0$ for problem (3.4). Since $\psi_1(x, y) = 0$ everywhere is a solution for this problem (see chapter 3), one concludes that $\psi_{1y}(x,0)=0$, which also satisfies matching. The remaining terms in (4.13) and (4.14b) then yield the result $h_0(x) = c_1x^{1/3}$. In this case, the free surface height is given by

$$\zeta(x) = c_1x^{\frac{1}{3}}\varepsilon+O\left(\varepsilon^2\right) \tag{4.15}$$

The vanishing of $\psi_1(x, z)$ means that, to the order ε, there is no interaction between the boundary layer and the core flow. The next step is to determine $\psi_2(x, z)$ and $h_1(x)$ by considering an analogous matching process to the above, using $m = n = 2$. Now applying E_2 on the outer expansion gives,

$$\begin{aligned} E_2\psi = {} & 3y^2-2y^3+6y\varepsilon h_0-6y^2\varepsilon h_0+6y\varepsilon^2h_1 \\ & -6y^2\varepsilon^2h_1+3\varepsilon^2{h_0}^2-6y\varepsilon^2{h_0}^2+\varepsilon\psi_1(x,y+\varepsilon h)+\varepsilon^2\psi_2(x,0). \end{aligned} \tag{4.16}$$

To apply H_2, the equation has to be written in terms of inner variable, $y = \varepsilon\eta$, which results in,

$$H_2E_2\psi = 3\left(y^2+2\varepsilon h_0y\right)+\varepsilon^2\left[\psi_2(x,0)+3h_0^2\right].$$

and

$$H_2\psi = 3\left(y + \varepsilon c_1 x^{1/3}\right)^2 = 3\left[y^2 + 2y\varepsilon c_1 x^{1/3} + \varepsilon^2\left(c_1 x^{1/3}\right)^2\right].$$

Therefore,

$$E_2H_2\psi = 3\left(y^2 + 2c_1\varepsilon y x^{1/3} + \varepsilon^2 c_1^2 x^{2/3}\right). \tag{4.17}$$

This yields the fact that $\psi_2(x, 0) = 0$ in the core expansion, concluding that $\psi_2(x, z) = 0$ everywhere, reflecting the absence of interaction between the boundary layer and the core flow also to order ε^2. The next step is to determine $h_1(x)$ and $\psi_3(x, 0)$. Upon using expressions (2.13), (2.21) and (2.27), for $n = m = 3$, one obtains

$$\begin{aligned} E_3H_3\psi = {} & 3y^2 - 2y^3 + \varepsilon y c_1 x^{1/3}[6 - 6y] \\ & + \varepsilon^2 x^{2/3}\left[3c_1^2 - 6c_1^2 y + c_2 y\right] + \varepsilon^3 x\left[c_2 c_1 - 2\left(c_1^3 - 1\right)\right]. \end{aligned} \tag{4.18}$$

Applying H_3E_3 to the outer expansion (3.2a) gives in turn:

$$\begin{aligned} H_3E_3\psi = {} & 3y^2 - 2y^3 \\ & + \varepsilon y h_0[6 - 6y] \\ & + \varepsilon^2\left[3h_0^2 + 6yh_1 - 6yh_0^2\right] \\ & + \varepsilon^3\left[6h_0h_1 - 2h_0^3 + \psi_3(x,0)\right]. \end{aligned} \tag{4.19}$$

Upon matching, the height of the free surface to the next order is determined, namely

$$h_1 = \frac{c_2}{6} x^{2/3} \tag{4.20}$$

Also, the boundary condition, which is required to complete the set of boundary conditions in (3.10b), is obtained. Thus,

$$\psi_3(x,0) = 2x. \tag{4.21}$$

Condition (4.21) yields $\lambda_3(x) = -2$ in (3.10b). Therefore, for the first time, a non-trivial outer problem is reached.

4.2 Free surface wall jet profiles

It can be concluded that the outer flow up to order ε^3, remains the same as the Newtonian flow. However, the important result reached here from the matching process is that the height of the free surface is given by

$$\zeta(x) = \varepsilon c_1 x^{1/3} + \varepsilon^2 \frac{c_2}{6} x^{2/3} \tag{4.22}$$

Figure 4.1 displays the dependence of free surface height on inertia. The surface profiles suggest a significant thickening of the film when inertia increases. It is evident from the expression of the free surface height (4.22), that its slope is singular at x = 0. For the surface to exhibit maximum, $\frac{d\zeta(x)}{dx} = 0$, resulting in $x_m = -\left(\frac{3c_1}{\varepsilon c_2}\right)^3$ In this case, c_1 and c_2 are constants and equal to 0.495, and -3 respectively. Therefore the surface exhibits a maximum at a location given by $x = \left[\frac{.495}{\varepsilon}\right]^3$. From (4.22) it is found that, close to the channel exit the theory is valid in the streamwise direction at a distance which is equal to one channel width. Again, far downstream the theory is valid in the streamwise direction at a distance which is of the same order of the Reynolds number. Figure 4.2 depicts the variation of surface curvature with inclination, ϕ, for ε = 0.1, 0.2, 0.3. It shows that the curvature increases with ϕ, reaching a maximum at an inclination, and decreasing rapidly as $\phi \to 90^\circ$. Figure 4.3 displays the asymptotic and numerical streamwise velocity profile based on the inner layer solution (2.31), along with the free surface height. Note that the difference between figure 2.7 and figure 4.3 is that, the free surface height was not yet obtained in figure 6, and this latter was drawn in the (η, x) plane.

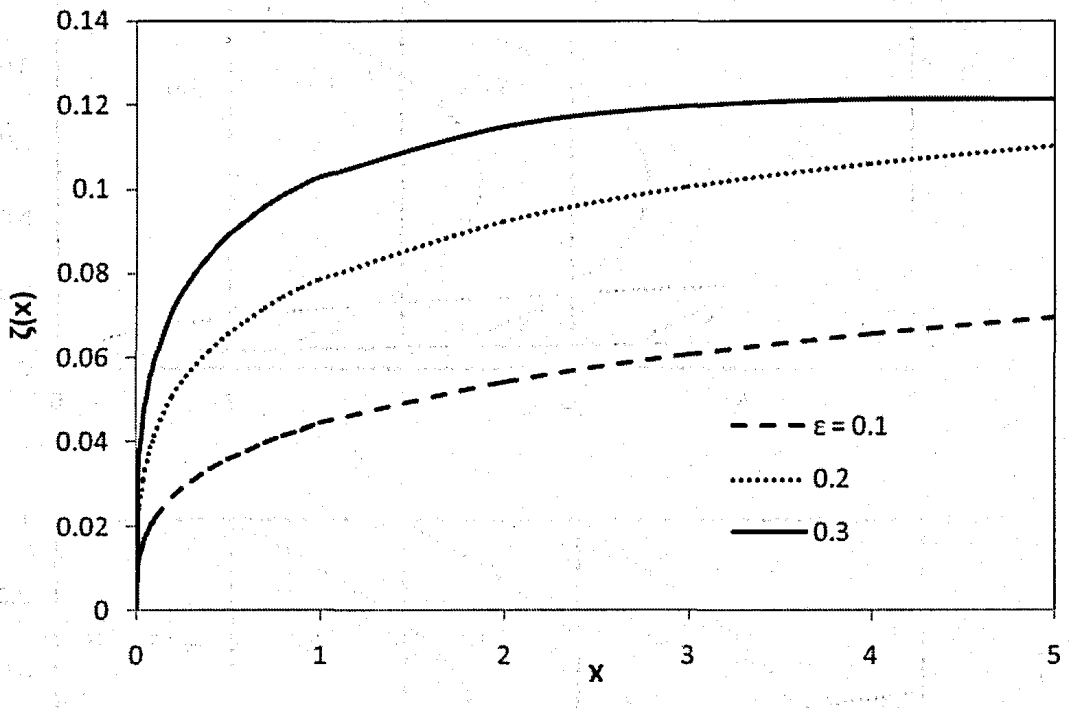

Figure 4.1. Dependence of the free surface height, ζ(x), on inertia.

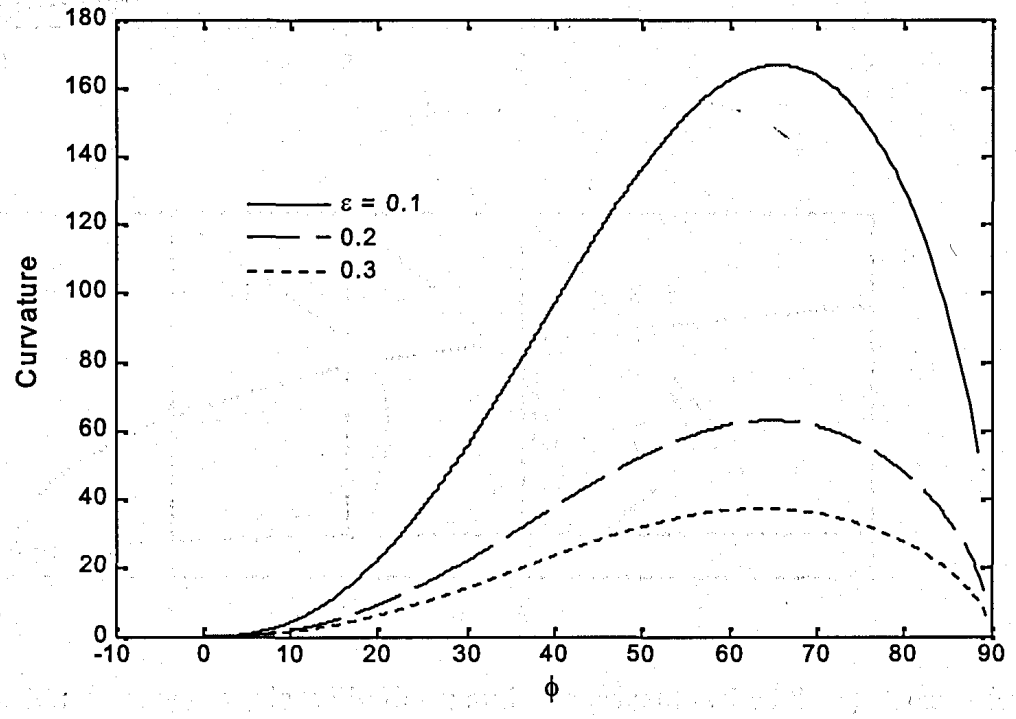

Figure 4.2. Variation of curvature vs. inclination ϕ along the free surface for ε =0.1, 0.2, 0.3

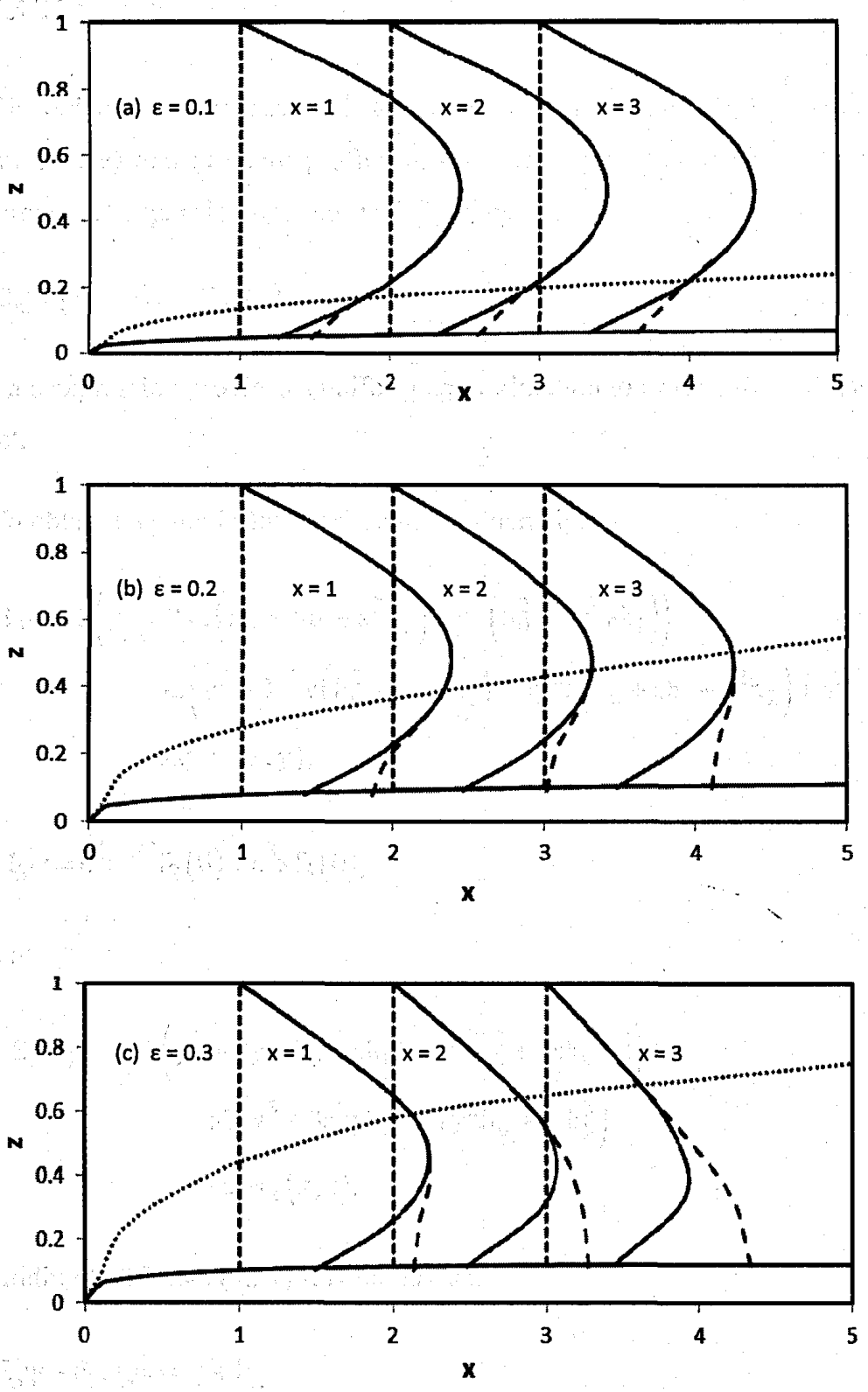

Figure 4.3: The asymptotic (solid lines) and numerical (dashed lines) streamwise velocity profiles for (a) ε = 0.1, (b) ε =0.2 and (c) ε =0.3. Note : u and x are drawn on the same scale. The vertical dashed line is the origin of u at each position.

4.3 The composite flow

The objective of this section is to find out the composite velocity profile (streamwise and transverse) and pressure profile outside the channel. Following Van Dyke (1964), the composite expansion operator is defined by

$$C_n \equiv (E_n + H_n - E_n H_n) \tag{4.34}$$

This expression provides a uniform approximation to order ε^n over the whole width of the jet.

To obtain $C_3\psi$ the followings are needed namely,

$$\begin{aligned} E_3\psi = 3\Big(y^2 + 2y\varepsilon\big(h_0 + \varepsilon h_1 + \varepsilon^2 h_2\big) + \varepsilon^2\big(h_0^2 + 2\varepsilon h_0 h_1\big)\Big) \\ -2\Big(y^3 + 3\varepsilon^2 y\big(h_0^2 + 2\varepsilon h_0 h_1\big) + 3y^2\varepsilon\big(h_0 + \varepsilon h_1 + \varepsilon^2 h_2\big) + \varepsilon^3 h_0^3\Big) \\ +\varepsilon^3\psi_3(x,y), \end{aligned} \tag{4.35}$$

$$H_3\psi = \varepsilon^2 x^{2/3} f_2(\theta) + \varepsilon^3 x f_3(\theta), \tag{4.36}$$

and

$$\begin{aligned} -E_3H_3\psi = -3\Big(y^2 + 2y\varepsilon(h_0 + \varepsilon h_1) + \varepsilon^2\big(h_0^2 + 2\varepsilon h_0 h_1\big)\Big) \\ +2\Big(y^3 + 3\varepsilon^2 y h_0^2 + 3\varepsilon y^2 h_0 + \varepsilon^3 h_0^3\Big) \\ -\varepsilon^3\psi_3(x,0). \end{aligned} \tag{4.37}$$

Adding (4.35) and (4.37) it is found that,

$$\begin{aligned} E_3\psi - E_3H_3\psi = 6y\varepsilon^3 h_2 \\ -2\Big(3\varepsilon^2 y(2\varepsilon h_0 h_1) + 3y^2\varepsilon\big(\varepsilon h_1 + \varepsilon^2 h_2\big)\Big) \\ +\varepsilon^3\psi_3(x,y) - \varepsilon^3\psi_3(x,0). \end{aligned} \tag{4.38}$$

Therefore, combining (4.36) and (4.38) $C_3\psi$ is obtained as following

$$\begin{aligned}
C_3\psi &= H_3\psi + E_3\psi - E_3H_3\psi = \varepsilon^2 x^{2/3} f_2(\theta) + \varepsilon^3 x f_3(\theta) \\
&\quad + 6y\varepsilon^3 h_2 - 2\left(6\varepsilon^3 y h_0 h_1 + 3y^2\varepsilon\left(\varepsilon h_1 + \varepsilon^2 h_2\right)\right) \\
&\quad + \varepsilon^3\psi_3(x,y) - \varepsilon^3\psi_3(x,0) \\
&= \varepsilon^2 x^{2/3} f_2 + \varepsilon^3 x f_3 + \varepsilon^3\psi_3(x,y) - \varepsilon^3\psi_3(x,0) + 6z\varepsilon^3 h_2 \quad \text{[conversion to z]} \\
&\quad - 2\left[6\varepsilon^3 z h_0 h_1 + 3(z - \varepsilon h_0)^2 \varepsilon^2 (h_1 + \varepsilon h_2)\right] \\
&= \varepsilon^2 x^{2/3} f_2 + \varepsilon^3\left[x f_3 + \psi_3(x,z) + 6z h_2 - \psi_3(x,0)\right] \\
&\quad - 2\left[6\varepsilon^3 z h_0 h_1 + 3\varepsilon^2\left(z^2 - 2\varepsilon z h_0\right)(h_1 + \varepsilon h_2)\right] \\
&= \varepsilon^2\left[x^{2/3} f_2 - 6z^2 h_1\right] \\
&\quad + \varepsilon^3\left[x f_3 + \psi_3(x,z) - \psi_3(x,0) + 6z h_2 - 6z^2 h_2\right]
\end{aligned} \tag{4.39}$$

or

$$\begin{aligned}
C_3\psi &= \varepsilon^2 x^{2/3}\left[f_2 - z^2 c_2\right] \\
&+ \varepsilon^3\left\{x f_3 + \psi_3(x,z) - 2x + \left[6z - 6z^2\right] h_2\right\}
\end{aligned} \tag{4.40}$$

Therefore the streamwise velocity expression becomes

$$\begin{aligned}
C_3 u &= \varepsilon x^{1/3} f_2' + \varepsilon^2 x^{2/3} f_3' - 12\varepsilon^2 z h_1 + \varepsilon^3\psi_{3z}(x,z) - \varepsilon^3\psi_{3z}(x,0) \\
&\quad + 6\varepsilon^3 h_2 - 12\varepsilon^3 z h_2.
\end{aligned} \tag{4.41}$$

Although the value of h_2 is required if the streamwise velocity is to be evaluated to $O(\varepsilon^3)$, this accuracy is not indispensible(absolutely necessary) when the flow variables are determined. This is the case, for instance, for the following expressions for the streamwise velocity component:

$$C_2 u(x,z) = \varepsilon x^{1/3} f_2' + \varepsilon^2 x^{2/3} f_3' - 12\varepsilon^2 z h_1 + O(\varepsilon^3)$$
$$= \varepsilon x^{1/3} f_2'(\theta) + \varepsilon^2 x^{2/3}\left[f_3'(\theta) - 2z c_2\right] + O(\varepsilon^3) \text{ as } h_1 = \frac{c_2}{6} x^{2/3} \tag{4.42}$$

The transverse velocity component can now be obtained from (4.40) using the method below. Note that, $\theta = \eta\xi^{-1/3} = \left(\frac{z}{\varepsilon} - h\right)x^{-1/3}$. As $f = f(\theta) = f(\xi,\eta)$, therefore,

$$f_x = f_\xi \xi_x + f_\eta \eta_x = f_\xi + f_\eta \eta_x = f_\theta \theta_\xi + \eta_x f_\theta \theta_\eta$$
$$= f'\left(-\frac{\eta}{3}\xi^{-4/3} + \eta_x \xi^{-1/3}\right) = -f'\left(\frac{1}{3}\xi^{-4/3}\left(\frac{z}{\varepsilon} - h\right) + h'\xi^{-1/3}\right) \tag{4.43}$$
$$= -f'\left(\frac{1}{3}\xi^{-1}\theta + h'\xi^{-1/3}\right) = -\left(\frac{1}{3\xi}(\theta + c_1) + \varepsilon h_1' \xi^{-1/3}\right) f'.$$

Using (4.43) in (4.40)

$$C_2\psi_x = \varepsilon^2 \frac{2}{3} x^{-1/3}\left[f_2 - z^2 c_2\right] + \varepsilon^2 x^{2/3} f_{2x} + \varepsilon^3 (f_3 + x f_{3x} + \psi_{3x} - 2)$$
$$= \varepsilon^2 \frac{2}{3} x^{-1/3}\left[f_2 - z^2 c_2\right] - \varepsilon^2 x^{2/3} f_2'\left(\frac{1}{3} x^{-4/3}\left(\frac{z}{\varepsilon} - h_0\right) + h' x^{-1/3}\right)$$
$$-\frac{\varepsilon^2}{3} x^{-1/3} z f_3'$$

$$C_2\psi_x = \varepsilon^2 \frac{2}{3} x^{-1/3}\left[f_2 - z^2 c_2\right] - f_2'\left(\frac{1}{3} x^{-2/3}\left(\varepsilon z - \varepsilon^2 h_0\right) + \varepsilon^2 h' x^{1/3}\right) - \frac{\varepsilon^2}{3} x^{-1/3} z f_3'$$
$$= -\frac{\varepsilon}{3} x^{-2/3} z f_2' + \varepsilon^2 \frac{2}{3} x^{-1/3}\left[f_2 - z^2 c_2\right] + f_2'\left(\frac{1}{3} x^{-2/3}\varepsilon^2 h_0 - \varepsilon^2 h_0' x^{1/3}\right) \tag{4.45}$$
$$-\frac{\varepsilon^2}{3} x^{-1/3} z f_3'$$
$$= -\frac{\varepsilon}{3} x^{-2/3} z f_2' + \frac{\varepsilon^2}{3} x^{-1/3}\left[2f_2 - z f_3' - 2z^2 c_2\right]$$

$$C_2\psi_x(x,z) = -\frac{\varepsilon}{3} x^{-2/3} z f_2' + \frac{\varepsilon^2}{3} x^{-1/3}\left[2f_2 - z f_3' - 2z^2 c_2\right] + O\left(\varepsilon^3\right) \tag{4.46}$$

As, $z = \varepsilon\left(\theta x^{1/3} + h\right) = \varepsilon\left(\theta x^{1/3} + h_0\right) + \varepsilon^2 h_1 = \varepsilon(\theta + c_1) x^{1/3} + \varepsilon^2 h_1$, therefore,

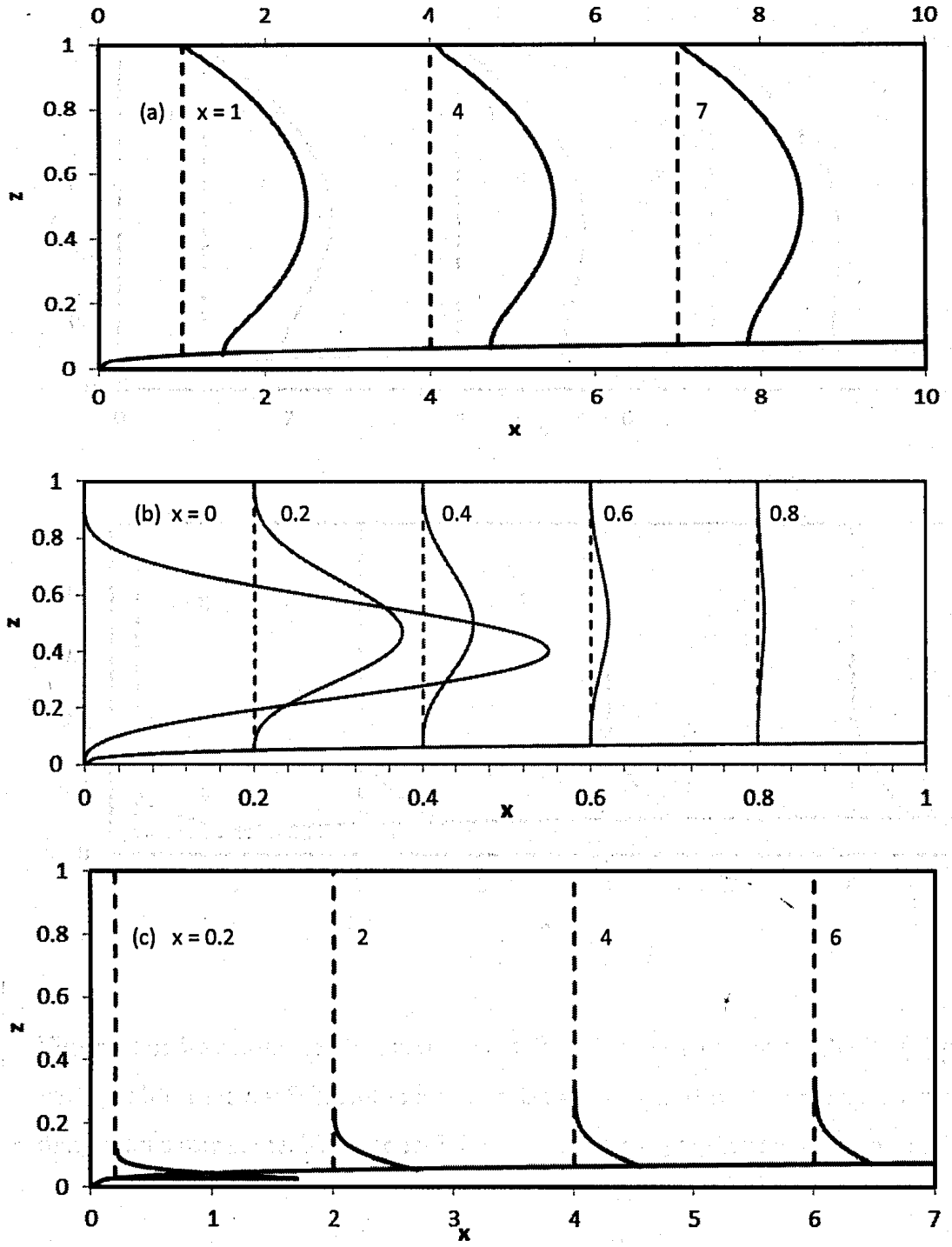

Figure 4.4: Variation of streamwise velocity (a), pressure (b) and transverse velocity (c) profiles with position for $\varepsilon = 0.1$. Note : streamwise velocity, pressure and transverse velocity are drawn on same scale. The vertical dashed line is the origin at each position.

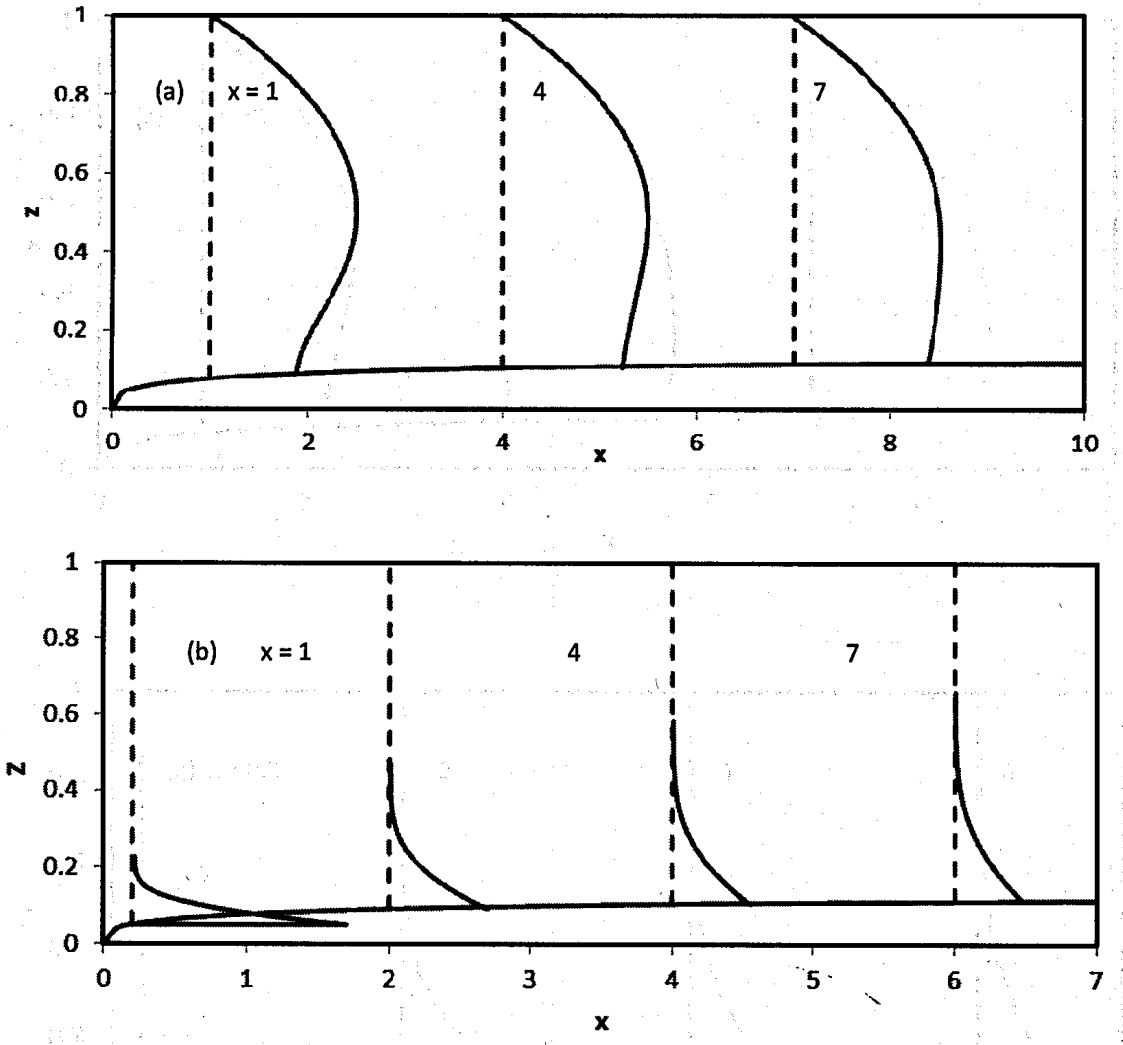

Figure 4.5: Variation of streamwise velocity (a), and transverse velocity (b) profiles with position for ε = 0.2. Note : streamwise velocity and transverse velocity are drawn on same scale. The vertical dashed line is the origin at each position.

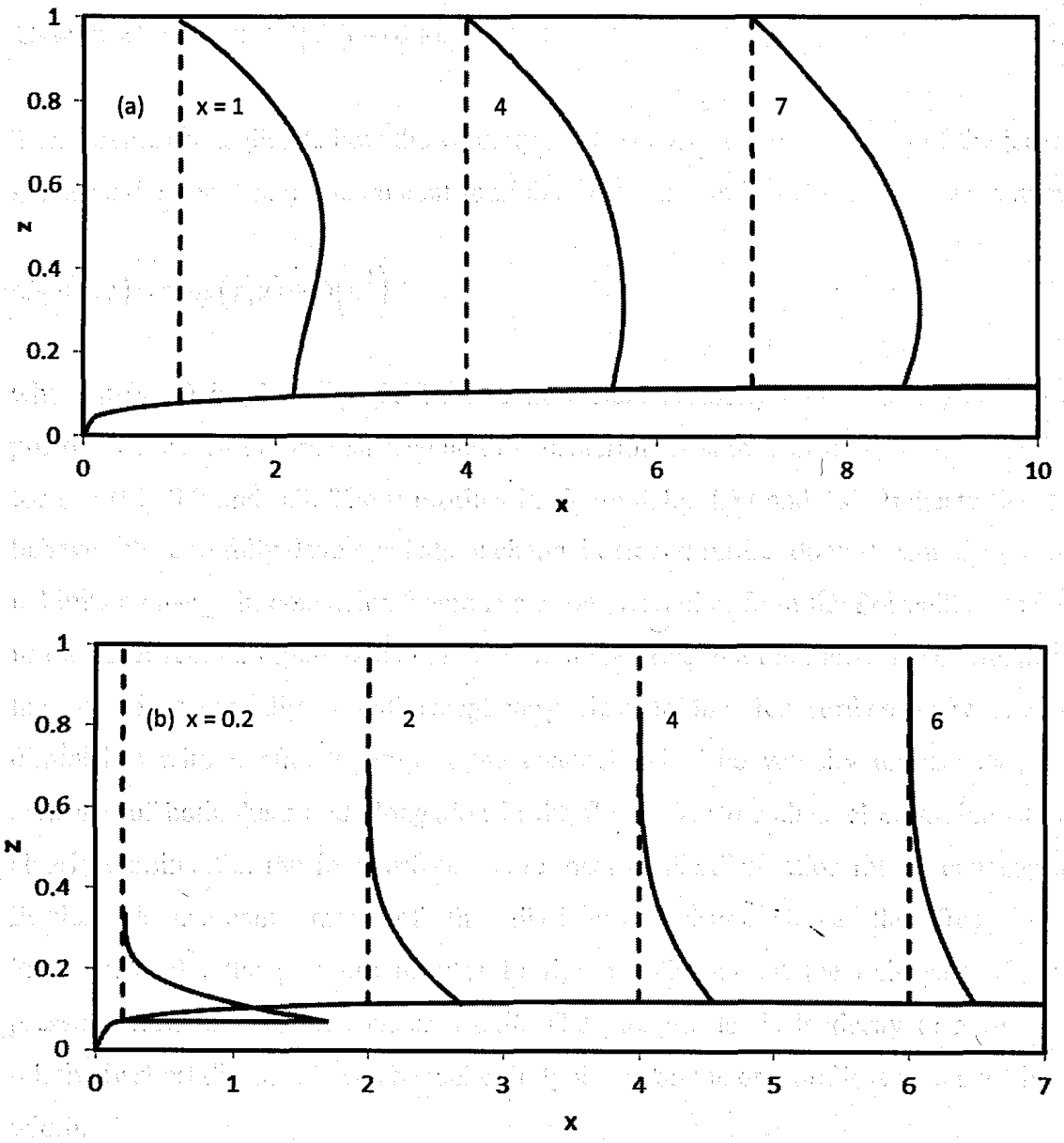

Figure 4.6: Variation of streamwise velocity (a), and transverse velocity (b) profiles with position for ε = 0.3. Note : streamwise velocity and transverse velocity are drawn on same scale. The vertical dashed line is the origin at each position.

$$C_2 w(x,z) = -\frac{\varepsilon^2}{3} x^{-1/3}\left[2f_2 - (\theta + c_1) f_2'\right] + O(\varepsilon^3) \tag{4.47}$$

These expressions dictate how the velocity profile changes over the width of the jet up to the second order. The non-zero contribution of pressure enters only to third order, namely

$$C_3 p(x,z) = \varepsilon^3 p_3(x,z) + O(\varepsilon^4), \tag{4.48}$$

where $p_3(x, z)$ is given by (3.24). The flow field (velocity and pressure) at different positions between the free surface and the centerline is shown in figure 4.4, 4.5 and 4.6, for ε = 0.1, 0.2 and 0.3. The u profiles in figure 4.4a, 4.5a and 4.6a indicate that flow behaves close to fully developed at the channel exit and further downstream, the u profile exhibits a change in concavity. There is a strong deviation from the Poiseuille behaviour in the inner region. Figure 4.3c, 4.4b and 4.5b confirms that the transverse component of the flow is essentially absent except very close to the free surface as w gradually diminishes with x after a jump at the channel exit. The velocity reflects the strong presence of both shear and elongation in the flow. Near the channel exit, elongation is clearly dominant at the free surface where most of the dissipation rate is concentrated. Further downstream, most of the dissipation occurs above the free surface. Simultaneously, the pressure profiles in figure 4.4b suggest the existence of strong pressure variation near the channel exit. The pressure tends to decay to zero over a relatively short distance from channel exit, typically on the order of less than one channel width.

4.4 Conclusion

In order to find out how the flow behaves outside the channel, matching was performed at the interface of the inner and core region. Van Dyke's (1964) matching rule was applied to obtain the boundary condition for the inner region and finally the free surface height was achieved. Again, composite matching rule was applied to find out the composite velocity profile (streamwise and transverse) and pressure profile outside the channel.

CHAPTER 5

5.1 Conclusion

The two-dimensional wall jet flow of a Newtonian fluid emerging from a channel is examined theoretically in this study. Following Tillett (1968) and other existing asymptotic analyses in the literature for laminar free surface flows, the method of matched asymptotic expansions is used to examine the free surface wall jet at high Reynolds number. For a recent perspective on asymptotic analyses, their applications and historic development, the reader is referred to the book by Sobey (2005) on interactive boundary layer and triple-deck theory. Similarly to all boundary layer analyses, where the solution is not valid within a small distance from inception such as very near a leading edge or a stagnation point (for an impinging jet), the analysis precludes the flow at the channel exit. However, the distance in question is small, on the order of the (local) boundary layer thickness. Consequently, the boundary layer approach turns out to be successful in capturing the flow nature near inception. The solution is developed in powers of ε, where ε^3 is the inverse Reynolds number. Special emphasis is placed on the effect of inertia on the shape of the free surface and the profiles of the velocity and pressure close to the exit.

The boundary layer structure near the free surface was examined in detail. The viscous relaxation length for diffusion of stress singularity was found, as expected, to increase with inertia, with a corresponding thinning in the boundary layer. The monotonically decreasing pressure profile typically predicted for a free jet (Tillett 1968) was also predicted for the free surface wall jet. Finally, the significance of the current study and the advantages of the proposed formulation cannot be overstated. In typical jet flow calculations in the literature, fully developed conditions are assumed at inception. The present work provides the correct conditions near exit, which are required to determine the jet structure further downstream.

5.2 Future work

If the jet becomes thin far downstream, a boundary layer formulation can be used with the presently predicted boundary conditions for steady and possibly transient flows (Khayat & Welke 2001, Muhammad & Khayat 2004). Note that the thin film approximation is not valid close to the exit; combined near and far field analyses must be used. This restriction applies even for thin jet emerging from channels and tubes. The current analysis can also be extended for particle removal from the work piece at higher impinging angle where the flow can be analyzed for complicated Poiseuille flow.

REFERENCES

BIN ZHAO, JEFFREY S. MOORE, DAVID J. BEEBE. 2001 Surface- directed liquid flow inside micro-channels. *Science* **291**, 1023 (2001).

DENIER, J. P. & DABROWSKI, P. P. 2004 On the boundary-layer equations for power-law fluids. *Proc. R. Soc. Lond. A*, **460**, 3143.

GLAUERT, M. B. 1956 The wall jet. *J. Fluid Mech.* 1, 625.

GOLDSTEIN, S. I960 *Lectures in Fluid Mechanics.* (Interscience, New York:).

GOREN, S. L. & WRONSKI, S. 1966 The shape of low-speed capillary jets of Newtonian liquids. *J. Fluid Mech.* **25**, 185.

HIGGINS, B. G. 1982 Downstream development of two-dimensional viscocapillary film flow. *Ind. Eng. Chem. Res.* **21**, 168.

http://news.cnet.com

http://www.notebooklist.net/asus-lenovo-and-more/acer-travelmate-8000-timeline-laminar-wall-jet.html

KHAYAT, R. E. & WELKE, S. 2001 Influence of inertia, gravity, and substrate topography on the two-dimensional transient coating flow of a thin Newtonian fluid film. *Phys. Fluids* **13**, 355.

MIDDLEMAN, S. & GAVIS, J. 1961 Expansion and contraction of capillary jets of viscoelastic liquids. *Phys. Fluids.* **4**(8), 963.

MUHAMMAD, T. & KHAYAT, R. E. 2004 Effect of substrate movement on shock formation in pressure-driven coating flow. Phys. Fluids **13**, 355.

MIYAKE, Y., MUKAI, E. & IEMOTO, Y. 1979 On a two-dimensional laminar liquid jet. *Bullt. Japan Soc. Mech. Eng.* **22**, 1382.

PASQUALI, M. & SCRIVEN, L.E. 2002 Free surface flows of polymer solutions with models based on the conformation tensor, *J. Non-Newtonian Fluid Mech.* **108**, 363

PHILIPPE, C. & DUMARGUE, P. 1991 Étude de l'établissement d'un jet liquide laminaire émergeant d'une conduite cylindrique verticale semi-infinie et soumis à l'influence de la gravité. *J. Appl. Math. Phys.* (*ZAMP*) **42**, 227.

RUSCHAK, K. J. & SCRIVEN, L. E. 1977 Developing flow on a vertical wall, *J. Fluid Mech.* **81**, 305.

SCHLICHTING, HERMAN. 1999. Boundary Layer theory.

SHI, J. M., BREUER, M. & DURST, F. 2004 A combined analytical–numerical method for treating corner singularities in viscous flow predictions. *Int. J. Num. Methods Fluids* **45**, 659

SMITH, F.T 1975 Flow through constricted or dilated pipes and channels: Part 1 *Q.Jl Mech. appl. Math.* **29**,343

SMITH, F.T 1975 Flow through constricted or dilated pipes and channels: Part 2 *Q.Jl Mech. appl. Math.* **29**,365

SMITH, F.T 1979 The separating flow through a severely constricted symmetric tube *J. Fluid Mech.* **90**,725

SOBEY, I. J. 2005 *Interactive boundary layer theory* (Oxford University Press, Oxford).

TILLETT, J. P. K. 1968 On the laminar flow in a free jet of liquid at high Reynolds numbers. *J. Fluid Mech.* **32**, 273.

TSUKIJI, T. & TAKAHASHI, K. 1987 Numerical analysis of an axisymmetric jet using a streamline coordinate system. *JSME Int. J.* **30**, 1406.

NORMAN ARNOLD TURNQUIST, MARK WILIAM KOWALCZYK, FARSHAD GHASRIPOOR. 2007 Use of spray coatings to achieve non-uniform seal clearances in turbomachinary. United States Patent No. 7,255,929 B2.

VAN DYKE, M. D. 1964 *Perturbation Methods in Fluid Mechanics*. (Academic Press, New York)

WATSON, E. 1964 The spread of a liquid jet over a horizontal plane. *J. Fluid Mech.* **20**, 481.

WILSON, D. E. 1986 A similarity solution for axisymmetric viscous-gravity jet. *Phys. Fluids* **29**(3), 632.

X. LIU, J. H. LIENHARD V. 1993 The hydraulic jump in circular jet impingement and in other thin films. *Experiments in Fluids* **15**, 108-116 (1993).

ZHANG XW, YAO ZH, HAO PF, XU HQ. 2002 Study on particle removal efficiency of an impinging jet by an image-processing method. *Experiments in Fluids* **32**(2002), 376-380.

ZHAO, J. & KHAYAT, R. E. 2007 Spread of non-Newtonian liquid jet over a horizontal plate. *J. Fluid Mech.* **613**, 411.

APPENDIX A

Asymptotic solution of $f_2(\theta)$

In this appendix, we follow Tillett's (1968) approach to determine the asymptotic solution.

From the equation of $f_2(\theta)$ in (2.22),

$$f_2''' + \frac{2}{3} f_2 f_2'' - \frac{1}{3} f_2'^2 = 0 \tag{A1}$$

where the boundary conditions are,

$$f_2(0) = f_2''(0) = 0 \tag{A2}$$

Setting $t = \theta + c$, where c is arbitrary, and

$$f_2(t) = \alpha t^2 + g(t) \tag{A3}$$

where α is a constant. The function αt^2 satisfies (A1) but not the boundary condition. From (A3),

$$f_2' = 2\alpha t + g',\ f_2'' = 2\alpha + g'',\ f_2''' = g''' \tag{A4}$$

Substituting (A4) into (A1) we get

$$g''' + \frac{2}{3}\alpha t^2 g'' - \frac{4}{3}\alpha t g' + \frac{4}{3}\alpha g + \frac{2}{3} g g'' - \frac{1}{3} g'^2 = 0 \tag{A5}$$

Omitting the quadratic terms from (A5) we get,

$$g''' + \frac{2}{3}\alpha t^2 g'' - \frac{4}{3}\alpha t g' + \frac{4}{3}\alpha g = 0 \tag{A6}$$

Two solutions of (A5) are $g = t$ and $g = t^2$. To find a third, Tillett set $g(t) = th(t)$. Therefore,

$$g' = h + th',\ g'' = 2h' + th'',\ g''' = 3h'' + th''' \tag{A7}$$

Substituting (A7) into (A6) we get the following,

$$h''' + \left(3t^{-1} + \frac{2}{3}\alpha t^2\right)h'' = 0 \tag{A8}$$

Let, $P(t) = 3t^{-1} + \frac{2}{3}\alpha t^2$ and $h'' = f$. Therefore (A8) can be written as,

$$f' + P(t)f = 0 \tag{A9}$$

$$e^{\int_0^t P(t)dt} f' + P(t)e^{\int_0^t P(t)dt} f = 0 \tag{A10}$$

$$\frac{d}{dt}e^{\int_0^t P(t)dt} = e^{\int_0^t P(t)dt}\frac{d}{dt}\int P(t)dt = P(t)e^{\int_0^t P(t)dt} \text{[From Leibniz theorem]} \tag{A11}$$

Substituting (A11) in (A10) we achieve the following,

$$e^{\int_0^t P(t)dt} f' + \frac{d}{dt}e^{\int_0^t P(t)dt} = 0$$

$$\frac{d}{dt}\left[e^{\int_0^t P(t)dt} f\right] = 0 \tag{A12}$$

$$e^{\int_0^t P(t)dt} f = \text{constant}$$

$$f = Ce^{-\int_0^t P(t)dt} = h''$$

Then,

$$\int P(t)dt = \frac{2}{9}\alpha t^3 \tag{A13}$$

Therefore the general solution of (A6) becomes,

$$g(t) = At^2 + Bt + Ce^{-\frac{2}{9}\alpha t^3}\left\{\frac{81}{4\alpha^2 t^6} + o(t^{-6})\right\} = 0 \tag{A14}$$

Taking A= B= 0, we get the asymptotic solution,

$$f_2(t) \sim \alpha t^2 + Ce^{-\frac{2}{9}\alpha t^3}\left\{\frac{81}{4\alpha^2 t^6}+\ldots\right\} \qquad \text{(A15)}$$

APPENDIX B

Method of separation of variables to obtain w_3

The following is a boundary value problem (3.10) that ranges in $-\infty \leq x \leq \infty$ and $0 \leq z \leq 1$:

$$\nabla^2 w_3 + \frac{2}{z - z^2} w_3 = 0, \tag{B1}$$

The boundary conditions are,

$$w_3(x,1) = 0,$$
$$w_3(x,0) = 0 \qquad \text{for} \qquad x < 0,$$
$$w_3 \quad \text{bounded as } |x| \to \infty.$$

Let the solution is $w_3(x,z) = -F(x)V(z)$ (B2)

The reason is $w_n(x,z) = -\psi_{nx}$

Therefore $w_{3x} = -F'V \quad w_{3xx} = -F''V$

And $w_{3z} = -FV' \quad w_{3zz} = -FV''$

Therefore from (B1)

$$-F''V - FV'' - \frac{2}{z - z^2} FV = 0$$

$$\frac{F''}{F} + \frac{V''}{V} = -\frac{2}{z - z^2}$$

$$\frac{F''}{F} = -\frac{V''}{V} - \frac{2}{z - z^2} = \lambda \tag{B3}$$

Therefore we form two ODE

$$F'' - \lambda F = 0 \tag{B4}$$

$$V'' + V\left(\lambda + \frac{2}{z - z^2}\right) = 0 \qquad \text{(B5)}$$

Now equation (B4) is an eigenvalue problem.

If $\lambda > 0$, the characteristic equation is $\Gamma^2 - \lambda = 0$

It has real and unequal roots. $\Gamma = \pm\sqrt{\lambda}$

For this linear ordinary differential equation with constant coefficients the solution is sought as,

$$F(x) = Ae^{\sqrt{\lambda}x} + Be^{-\sqrt{\lambda}x}$$

To keep the solution bounded set B = 0 and thus we obtain, $F(x) = Ae^{\sqrt{\lambda}x} = Ae^{\beta_n x}$ taking $\lambda = \beta_n{}^2$

For n number of values of λ there are corresponding solution of F and V. Therefore from equation (B2),

$$w_3(x,z) = -F(x)V(z) = -\sum_{n=1}^{\infty} F_n(x)V_n(z) = -\sum_{n=1}^{\infty} A_n e^{\beta_n x} V_n(z) \qquad \text{(B6)}$$